

國立交通大學

資訊科學與工程研究所

碩士論文

自動建構在無偏頗三維量度
空間中的磁振造影腦模板

Automated Construction of MRI Brain Templates in
Unbiased Stereotaxic Space

研究生：張煙玉

指導教授：陳永昇 博士

中華民國九十七年八月

自動建構在無偏頗三維量度
空間中的磁振造影腦模板
Automated Construction of MRI Brain Templates in
Unbiased Stereotaxic Space

研究生：張煙玉

Student : Yen-Yu Chang

指導教授：陳永昇

Advisor : Yong-Sheng Chen



Computer Science

August 2008

Hsinchu, Taiwan, Republic of China

中華民國九十七年八月

摘要

在人腦分析研究中，腦模板對於提供一個標準座標空間是不可或缺的。藉由人腦空間正規化 (spatial normalization)，將腦部磁振造影 (MRI) 對應到腦模板的標準空間中，可對應出腦部功能與結構資訊。並且，將不同受試者的腦部磁振造影對應到同一標準空間中，才能進行合理的統計分析和比較。MNI305 和 ICBM152 是目前被廣泛使用的腦模板，然而因為不同研究群 (study group) 的腦部結構差異性，例如不同種族、性別和年齡的腦部結構差異，利用非此研究群所建立的腦模板進行空間正規化會導致對位 (registration) 的不精準性，因此，自定義模板 (customized template) 對於特定研究群的腦部分析中是必須的。因此，我們提出了一個自動化建立腦模板的方法，基於不需人工定義重要結構 (landmark) 自動化的流程，本方法可用於建造標準腦模板或自定義腦模板，此外，所建立之腦模板與研究群為無偏頗的 (unbiased)。

論文的主要內容是有關腦模板的建立方法。首先，我們利用一現有的工具—Non-uniform intensity Normalization (N3) 來校正腦部磁振造影的影像亮度不均勻性 (nonuniformity)。從研究群中挑選一個參考腦，此參考腦具有最小方差的非線性形變量度 (nonlinear deformation magnitude)。接著我們利用參考腦與其他受試者的腦部磁振造影來計算一個屬於此研究群的無偏頗空間 (unbiased space)，最後，將研究群中所有腦經過對位到此無偏頗空間後作平均，以建立無偏頗的腦模板。此外，藉由使用 MNI 腦模板作為媒介，我們也提供了自所建立的腦模板自動化對應到 Talairach 空間的座標轉換。

我們的研究中，提出了一個自動化建構無偏頗腦模板的流程。在實驗中證明了，使用研究群所建立的腦模板確實能減少空間正規化所造成的形變量，無偏頗的腦模板與研究群之間的變異亦減少，此外也提升了對位的準確性。

誌謝

感謝陳永昇老師和陳麗芬老師兩年的辛苦指導，老師不僅在課業上帶領我作研究，更在我低潮時給我支持和打氣，研究所這兩年有老師的指導實在非常幸運。也要感謝我身邊的朋友和實驗室同學，不論是一起玩耍、一起跑跑、一起唱歌還是一同作研究的朋友，有你們的陪伴，讓我度過了快樂的兩年。

最要感謝的是我的家人和男友，家人永遠是我動力的來源和精神上的支柱。謝謝可愛的男友無微不至的照顧和陪伴，身邊有你們讓我覺得自己是個幸福的研究生，謝謝你們！



Automated Construction of MRI Brain Templates in Unbiased Stereotaxic Space

A thesis presented

by

Yen-Yu Chang



Institute of Computer Science and Engineering

College of Computer Science

in partial fulfillment of the requirements

for the degree of

Master

in the subject of

Computer Science

National Chiao Tung University

Hsinchu, Taiwan

2008

Automated Construction of MRI Brain Templates in Unbiased Stereotaxic Space

Copyright © 2008

by

Yen-Yu Chang



Abstract

In brain diagnosis, brain template coordinate system, which serves a standard stereotactic space, is indispensable to providing a common space for pathology detection in individuals or groups. Inter-subject brain comparison can be achieved by registering different MR images to the standard space. Furthermore, it also guides algorithms for knowledge-based image labeling by registering individual brain to the template space containing a set of anatomical and functional labels annotated at specific coordinates. There are many widely-used templates, such as MNI305 and ICBM152. However, normalizing brains to these templates arbitrarily may cause structure artifact due to large spatial distortion. Therefore, a customized brain template is necessary for structure brain analysis for specific study group. We proposed an automatic procedure to create the study-specific brain templates. This non-manual and automatic process provides a convenient and efficient method to generate templates without manual landmark-definition artifact.

In this study, we develop associated algorithms to automatically construct MRI brain templates from a database containing brain MRI volumes of Taiwanese for both genders. First, we use Non-parametric Non-uniform intensity Normalization (N3) technique to correct the nonuniformity of image. We choose a brain volume, which is one subject of the image set and has the minimum variation of deformation magnitude to the other subjects, as the representative brain. Thirdly, we compute the unbiased space according to the representative brain and all other brain images. Finally, we normalize all images to the unbiased space and average them to generate the brain template. Otherwise, we provide the automatic transformation from the created template to Talairach coordinate system by using the MNI template as the bridge to Talairach space.

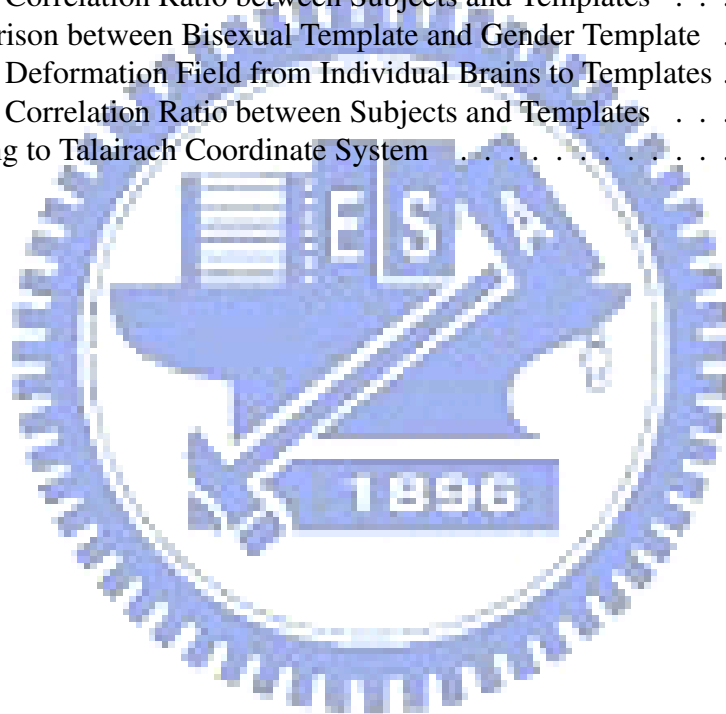
In this work, we proposed an automatic procedure of brain template construction. We demonstrate that the constructed study-specific brain templates can reduce the amount of spatial distortion of normalization and improve the registration accuracy.



Contents

List of Figures	v
List of Tables	vii
1 Introduction	1
1.1 Background	2
1.1.1 Magnetic resonance imaging (MRI)	2
1.1.2 Brain Template	2
1.2 Procedure of Template Construction	8
1.3 Thesis Scope	11
1.4 Thesis Organization	12
2 Template Construction Method	13
2.1 Introduction	14
2.2 Nonuniformity Correction	15
2.3 Image Registration	16
2.4 Selection of Representative Brain	18
2.5 Determination of Unbiased Stereotaxic Space	18
2.6 Average Template in Unbiased Space	22
2.7 Brain Tissue Templates	22
2.8 Mapping to Talairach Coordinate System	24
3 Template Evaluation Method	27
3.1 Introduction	28
3.2 Nonlinear Deformation Field between Subjects and Templates	28
3.2.1 Magnitude of Deformation Field	28
3.2.2 Variance of Deformation Field	29
3.3 Similarity between Registered Subjects and Templates	30
4 Experiment Results	31
4.1 Materials	32
4.2 Construction of Brain Templates	33

4.2.1	Nonuniformity Correction	33
4.2.2	Selection of Representative Brain	33
4.2.3	Determination of Unbiased Stereotaxic Space	38
4.2.4	The Unbiased Average Templates	38
4.3	Evaluation of Brain Templates	44
4.3.1	Nonlinear Deformation Field	44
4.3.2	Similarity between Registered Subjects and Templates	51
4.4	Mapping to Talairach Coordinate System	57
5	Discussion	61
5.1	Comparison between Unbiased Template and ICBM152	62
5.1.1	Deformation Field from Individual Brains to Templates	62
5.1.2	Correlation Ratio between Subjects and Templates	64
5.2	Comparison between Bisexual Template and Gender Template	65
5.2.1	Deformation Field from Individual Brains to Templates	65
5.2.2	Correlation Ratio between Subjects and Templates	67
5.3	Mapping to Talairach Coordinate System	67
6	Conclusions	69
	Bibliography	71



List of Figures

1.1	Brodmann map	5
1.2	Talairach atlas	7
1.3	MNI305 and ICBM152 templates	8
2.1	Flow chart of template construction	15
2.2	Nonuniformity of MR images	16
2.3	Affine registration and nonlinear registration	17
2.4	The sketch map of selection of the representative brain	19
2.5	The sketch map of transforming representative brain to the unbiased space	20
2.6	The sketch map of interpolating the mapping coordinate in the unbiased space	21
2.7	Flow chart of average template construction	23
2.8	Flow chart of tissue templates construction	24
4.1	Results of nonuniformity correction using SPM and N3	34
4.2	Results of nonuniformity correction using SPM and N3	35
4.3	The selected representative brain	37
4.4	The representative brain and the unbiased space	39
4.5	The 191 average template and the tissue templates	41
4.6	The 191 average template, the prime template and the gender templates	42
4.7	The brain templates for each age groups	43
4.8	The distribution of nonlinear deformation magnitude to Unbiased Template and ICBM152 template	46
4.9	The distribution of nonlinear deformation variance to Unbiased Template and ICBM152 template	47
4.10	Nonlinear deformation magnitude of 65 elder subjects to prime-age unbiased template and ICBM152 template	48
4.11	Nonlinear deformation variance of 65 elder subjects to prime-age unbiased template and ICBM152 template	49
4.12	The distribution of nonlinear deformation magnitude to the bisexual template and the male template	52

4.13	The distribution of nonlinear deformation variance to the bisexual template and the male template	53
4.14	The distribution of nonlinear deformation magnitude to the bisexual template and the female template	54
4.15	The distribution of nonlinear deformation variance to the bisexual template and the female template	55
4.16	The position of five landmarks in Talairach atlas	58
4.17	The position of landmarks in our template space	59
4.18	The mapping position of landmarks from Talairach to our template space . .	60



List of Tables

4.1	Number of subjects in our database	32
4.2	Number of subjects of candidates for representative brain	36
4.3	Number of subjects in each age group	36
4.4	Number of subjects for construction of prime template and gender template	40
4.5	The mean and variance magnitude of nonlinear deformation comparing Unbiased template v.s. ICBM152	45
4.6	The mean and variance magnitude of nonlinear deformation comparing prime-age unbiased template v.s. ICBM152	45
4.7	Number of subjects for construction of bisexual template and gender tem- plates	50
4.8	The average magnitude of nonlinear deformation comparing Bisexual tem- plate, Male template, and Female template	51
4.9	The variance of nonlinear deformation magnitude comparing Bisexual tem- plate, Male template, and Female template	51
4.10	The average correlation ratio to 191 average template and ICBM152 template	56
4.11	The average correlation ratio to Bisexual average template and gender tem- plates	56
4.12	Labeled position of landmarks	57
4.13	Labeled position of landmarks	58



Chapter 1

Introduction



1.1 Background

1.1.1 Magnetic resonance imaging (MRI)

Magnetic resonance imaging (MRI) is primarily a medical imaging technique most commonly used in visualizing the structure of organisms. It provides detailed images of the body in any plane without physically intrusion. MRI provides great contrast between the different soft tissues of the body, making it especially useful in neurological (brain), musculoskeletal, cardiovascular, and oncological imaging.

A magnetic resonance imaging instrument uses powerful magnets to polarize and excite hydrogen nuclei in water molecules in human tissue, producing a detectable signal which is spatially encoded resulting in images of the body. One advantage of an MRI scan is that it is harmless to the patient. It uses strong magnetic fields and non-ionizing radiation in the radio frequency range. Compare this to CT scans and traditional X-rays which involve doses of ionizing radiation and may increase the risk of malignancy. However, a disadvantage of MRI scanner is that the instrument is quite expensive. A new 1.5 tesla scanner approximately costs one million US dollars and two million US dollars for a new 3.0 tesla scanners. Construction of MRI suites can cost hundred thousand US dollars.

Nowadays, MRI is used extensively in applications of medical diagnosis. More and more researches focus on 3D stereo volume constructed by MRI scanner. For instances, brain functional localization and 3D digital brain development.

1.1.2 Brain Template

In brain diagnosis and its related works, the relationship of brain-imaging measurements between different subjects is necessary to be defined. Because there exists a high

individual variability in brain morphology, there is no reason to simply compare the same voxel in different brain volume. Even a same subject but in different orientation and position on MRI scanner, the same voxel of diverse brain images do not hold the same brain structure. For this reason, a standard stereotactic space, said a brain template coordinate system, is indispensable to providing a common space for pathology detection in individuals or groups [31] [10].

Brain atlases are also an important tool used in teaching and for inter-individual comparison and diagnostics of abnormal anatomical variations [20]. They can also guide algorithms for knowledge-based image analysis, automatic structure extraction [19], image labeling [7], and tissue classification [34] [32].

Due to the anatomic variability between individual brains, any atlas based on a single subject's anatomy cannot fully succeed. A probabilistic atlas may rectify this problem since it retain quantitative information on inter-subject variations in brain architecture. Initial approaches of the probabilistic atlas base on intensity averaging of pre-registered brains of a large group of subjects, such as the atlas of International Consortium of brain Mapping (ICBM) [21]. However, most of the anatomical variability in a normal brain is in the cortical surface and gyral patterns [3] and the cortical surface structure plays an important role in functional brain mapping. As a result, there are more surface-based brain atlases in recent years. In the study of Thompson et al. [30], the probabilistic surface atlas have been proven helpful in neuroscience studies. In 2005, Van Essen [33] developed a Population-Average, Landmark- and Surface-based (PALS) atlas of human cerebral cortex. The PALS-B12 atlas was derived from 12 normal young adults. After accurate cortical surface reconstruction for each hemisphere, a target atlas was generated by averaging selected landmark contours from each of the 24 hemispheres. Then each individual hemisphere was deformed to this target by surface-based registration, where six landmarks were used, and formed the population-average surface.

Once having a standard brain structure space, inter-subject brain comparison can be achieved by registering different MR images to the standard space. Nevertheless, registration leads to the volume deformation. Inaccuracy of brain registration will increase when the template which causes larger deformation and distortion is applied [22] [4] [11]. Currently, the Talairach brain based on dissection of an 60-year-old French female's brain is a commonly used brain atlas. However, due to the complex brain structure variability of human population, a single brain atlas may not accurately represent every brain. [25] [20]. Further, the template created by the Montreal Neurological Institute (MNI) based on 152 western adult MR images is accepted as a standard by the International Consortium for Brain Mapping (ICBM) [21]. Nevertheless, the inter-ethnic difference of brain structure is confirmed in the study of Zilles et al. [35]. Their study revealed that the Japanese brains are shorter and wider than European brains. In the following paragraph, we will elucidate these commonly used brain templates.

Brodmann Map

Brodmann Map which defined the cerebral cortical areas, based on its cytoarchitecture, or organization of cells by Korbinian Brodmann(1868-1918), in 1909. Brodmann defined the cerebral cortex into 52 distinct regions from their cytoarchitectonic characteristics. These areas are now referred to as Brodmann areas. Many of the Brodmann areas based on their neuronal organization have since been correlated closely to diverse cortical functions. For example, area 4 is the primary motor cortex, and areas 41 and 42 correspond closely to primary auditory cortex. Although Brodmann Map have been discussed, debated, and renamed exhaustively for about a century, it remain the most widely known and cited cytoarchitectural organization of the human cortex. In Fig. 1.1, the 52 brodmann areas are shown.

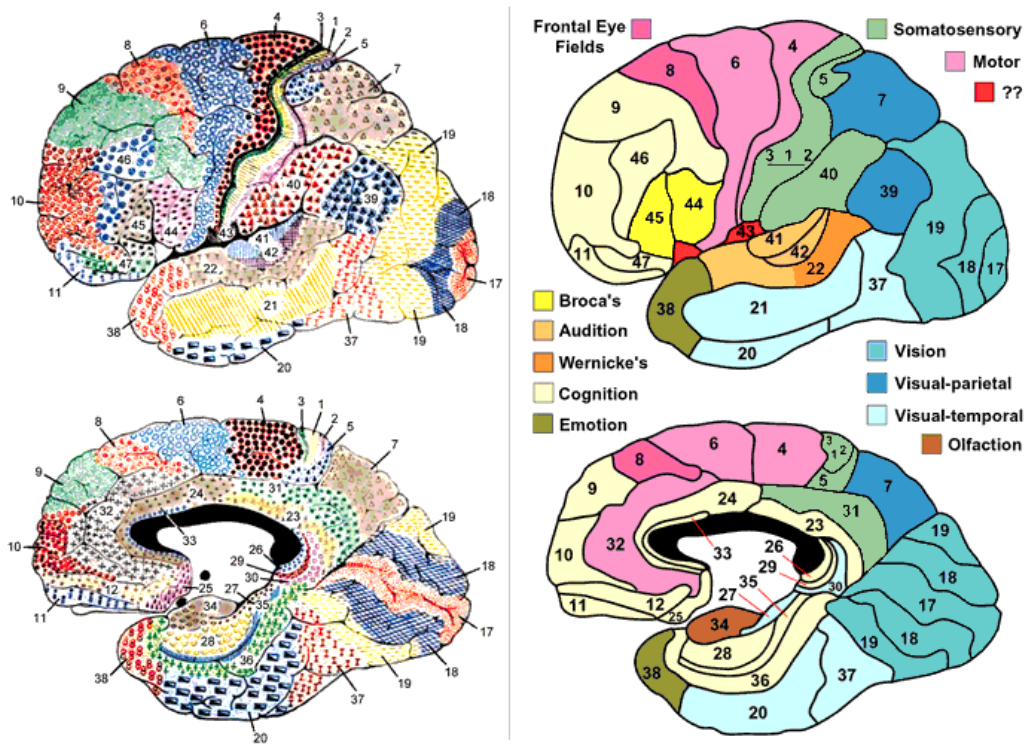


Figure 1.1: **Brodman map.** Brodmann map was defined based on its cytoarchitecture and numbered by Korbinian Brodmann in 1909. It was divided into 52 distinct regions which was called Brodmann areas. A Brodmann area was considered as a neuronal organization which may active for the same function. Many of the areas Brodmann defined based solely on their neuronal organization have since been correlated closely to diverse cortical functions.

(Graphic source : <http://spot.colorado.edu/~dubin/talks/brodman/brodman.html>)

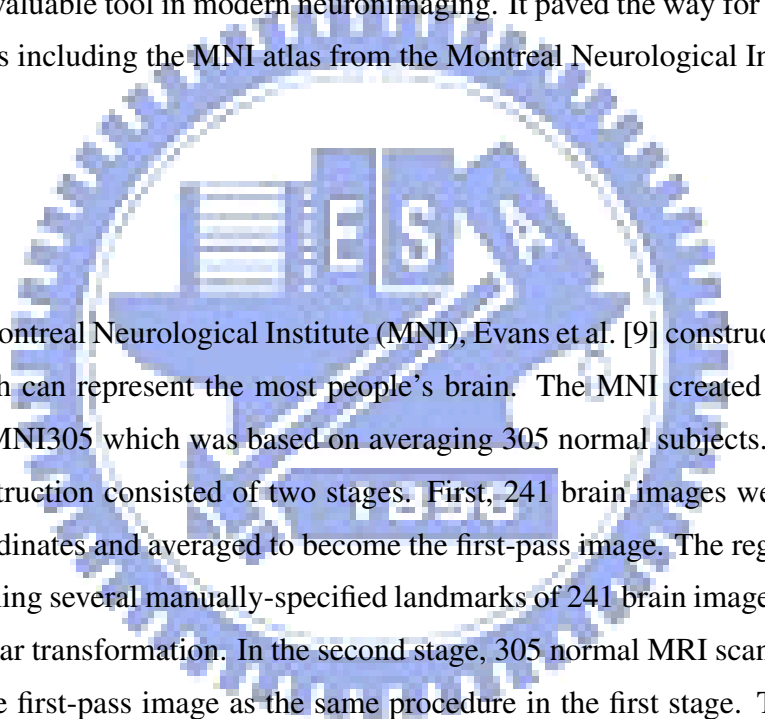
Atlas of Talairach and Tournoux

In 1988, Talairach and Tournoux [28] introduced a stereotaxic atlas of the human brain based on dissection of an 60-year-old French female's brain. They defined a standard coordinate system on this brain by making two points, the anterior commissure(AC) and posterior commissure(PC), lie on a straight horizontal line. Since AC and PC are both lie on midsagittal plane, the coordinate system is completely defined by requiring this plane to be vertical. Distances in Talairach coordinates are measured from the AC as origin. Talairach coordinate system approximately labels the Brodmann area based on visual inspection. In

other words, the location of brain structures in Talairach coordinate can be described according to the related Brodmann area. Fig 1.2 shows four slices of verticofrontal sections in Talairach atlas.

However, there are still some disadvantages of Talairach coordinate atlas. First, the brain examined for atlas creation was a 60-year-old French woman with a smaller than average cranium cannot be a good representative of human brain. Additionally, the assumption of perfectly symmetry in Talairach brain seems irrational. Nonetheless, the Talairach atlas is still an invaluable tool in modern neuronimaging. It paved the way for subsequently brain atlas studies including the MNI atlas from the Montreal Neurological Institute.

MNI305



In 1994, in Montreal Neurological Institute (MNI), Evans et al. [9] constructed a population-based atlas which can represent the most people's brain. The MNI created a MRI brain template called MNI305 which was based on averaging 305 normal subjects. The process of MNI305 construction consisted of two stages. First, 241 brain images were registered to Talairach coordinates and averaged to become the first-pass image. The registration was achieved by aligning several manually-specified landmarks of 241 brain images together by 9 parameters linear transformation. In the second stage, 305 normal MRI scans were linearly normalized to the first-pass image as the same procedure in the first stage. Their average was computed to obtain the MNI305 template, which is the first template constructed by MNI. Fig. 1.3(a) shows the three different views of the MNI305 template.

ICBM152 and ICBM452

In 2001, the International Consortium for Brain Mapping (ICBM) used 152 normal subject MR scans to construct a template, called ICBM152 [21]. The 152 normal brains

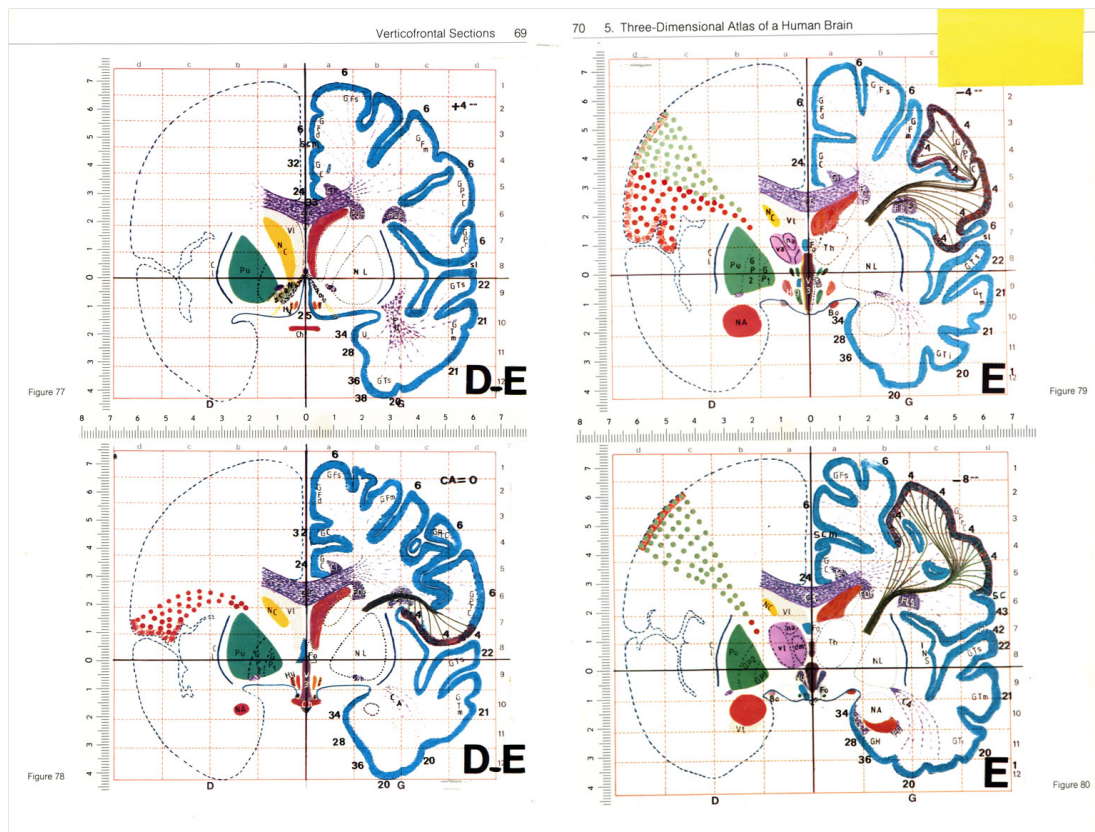


Figure 1.2: **Talairach atlas.** Talairach atlas of the human brain was introduced in 1988 by Talairach and Tournoux [28]. They defined a standard coordinate system based on dissection of an 60-year-old French female's brain. The Talairach atlas of anatomy constructed initially for stereotactic and functional neurosurgery is also used in human brain mapping, neuroradiology, medical image analysis, and neuroscience education. This figure shows four slices of verticofrontal sections in Talairach atlas.

(Graphic source : <http://homepages.nyu.edu/~ef725/amygdala.html>)

were registered to the MNI305 template using nine-parameter affine-transformation and averaged. These images were acquired at a higher resolution than the original 305 data of MNI305 due to advances in imaging technology. The ICBM152 template has been incorporated into several widely used functional images analysis software packages, such as SPM, AFNI and FSL. Fig. 1.3(b) shows the three different views of the ICBM152 template.

Afterward the ICBM created the ICBM452 template, which is a averaged of T1-weighted MRIs of normal young adult brains. The space the atlas is in is not based on any single

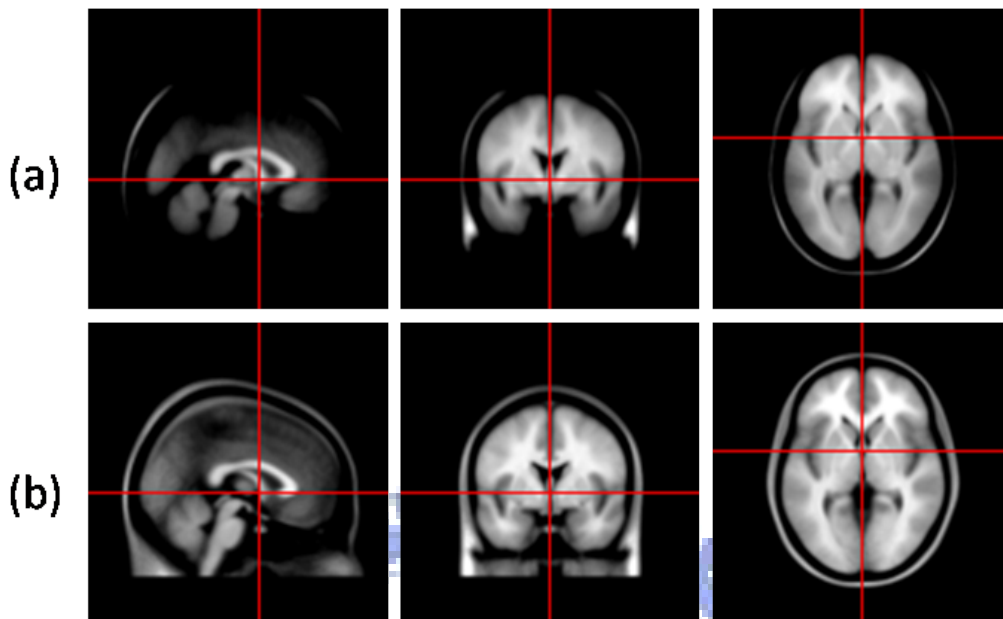


Figure 1.3: **MNI305 and ICBM152 templates.** (a) The MNI305 template was constructed by Montreal Neurological Institute (MNI) based on averaging 305 normal subjects. (b) The ICBM152 template was constructed by the International Consortium for Brain Mapping (ICBM) used 152 normal subject MR scans. These images were acquired at a higher resolution than the original 305 data of MNI305. ICBM152 template has been incorporated into several widely used functional images analysis software packages. (Graphic source : http://www.bic.mni.mcgill.ca/cgi/icbm_view/)

subject, instead, an average space constructed from the average position, orientation, scale, and shear from all the individual subjects. ICBM452 is not yet widely used.

1.2 Procedure of Template Construction

There are various methods of template construction. We roughly divide these methods into two categories, manual procedures and automatic procedures. Intuitively, manual procedures include manual landmark selection in template construction process contrary to automatic procedures. For example, MNI305 construction is a manual procedure. It

involved affine registration which achieved by aligning several manually-specified landmarks.

Nowadays, with the progress of MR imaging and registration technique, fully computerized registration has outstanding performance. Therefore, several automatic methods of template construction have been developed. In the following paragraph, we will give a brief introduction to various studies about template construction.

Japanese Template

In 2003, Sato, Yaki, Fukuda, and Kawashima [23] collected 1547 normal and right-handed Japanese subjects including 772 men and 775 women between the ages of 16 and 79 years. In order to evaluate age-related structural changes of cerebral hemispheres, they divided subjects into 10 groups according to age and sex. The construction contained two stages. First, an brain of each group, which has the least deviation in brain shape with respect to the database, was selected as the reference subject in the group. All selected brains were spatially normalized to Talairach space using global scaling model. In second step, all brains in a group were normalized to the selected reference brain. These transformation matrices defined the average size and shape of the brains. Then, the reference brain transformed to the average shape and size in this group by this transformation. Finally, the transformed brain was determined as reference (standard) brain of this age-sex group.

Korea Template

In 2005, 78 normal right-handed volunteers, including 49 males and 29 females, were recruited by Lee et al. [17] for the template construction. They were divided into 4 groups according to their genders (female and male) and ages (young and elderly). Two optimal

target brain of the templates for gender group were selected by manual method. They defined anterior commissure, posterior commissure, verticofrontal, and mid-sagittal planes by experts. The candidates of target brain in each group was determined by calculation of difference between these features. Subsequently, final selection of the target brains was conducted by experts manually. All brain images were normalized to the target brains of their gender group to form the four templates.

Human Cerebellum Template

Diedrichsen J. et al. [8] adopted an automatic template construction procedure to present a new high-resolution atlas template of the human, cerebellum and brainstem, in 2006. They claimed that the atlas is spatially unbiased, that is, the location of each structure is the expected location of that structure across individuals in MNI space. For any particular structure i in the template should be equal to the average, or expected, location of that structure across all individuals n :

$$E(y_i^{(n)}) = z_i, \quad \forall i \in \text{brainarea.}$$

They used Colin27 brain as the reference brain to generate the unbiased cerebellum template. Each individual images were averaged in the space defined by Colin27, then the average image applied the average deformation field to conduct the unbiased space. Compared to the normalization to the MNI whole-brain template, their method significantly improves the alignment of individual fissures, reducing their spatial spread by 60%, and improves the overlap of the deep cerebellar nuclei.

Neonatal Template

In 2007, Kazemi et al. [15] created a neonatal atlas template of newborns by an automatic procedure. Their procedure shares some of the techniques used in the approach

presented by Diedrichsen J. et al. [8]. First, all images were affine registered to the reference image, which is an arbitrary individual of brain images. The images resulting from the affine alignment are normalized to the reference image using nonlinear registration and resulted a average deformation field. Then the deformation field was applied to every brain images after nonlinear registered to the reference brain. Finally, the average brain template is calculated by averaging all transformed images. They repeated above process twice by replacing the reference image by the first pass template in order to minimizing the influence of the reference image.

They evaluated their template by anatomical local variation and amount of local deformations of brain tissue with adult and pediatric templates. It was shown that using the neonatal template results in better performance as indicated by reduction of deviation of anatomical equivalent structures.

1.3 Thesis Scope

In this thesis, we provide an automatic procedure of MRI brain template construction. This non-manual and automatic process provides a convenient and efficient method to generate a study-specific template without artifact. The intuition of constructing a template is simply averaging all brain volumes and resulting the average brain to be the template. Nevertheless, due to the different brain size, orientation and structure organization, the average image is inevitably too blurred to provide any information. Therefore, a common reference space must be defined so as to transform all brain images to this space before averaging.

Determination of the common reference space, however, is still an issue. We could use the MNI305 or ICBM152 templates, the widely-used templates, as our reference brain forthrightly. But because of Asian brain recruited in our study and the inter-ethnic dif-

ference of brain structure [35], we replace these widely-used templates with a optimal reference image within our brain database. After selection of reference image, called representative brain, we adopt the argument, introduced by Diedrichsen J. et al. [8], to create an unbiased space. Finally, all images are transformed to this unbiased space and averaged to result the template.

Furthermore, in order to quantitatively evaluate the generated template in comparison with ICBM152, we perform some evaluation experiments. Evaluations include study of amount of local deformations of brain tissues and the registration accuracy. On the other hand, we use the same evaluation method to verify the performance of the study specific template for both genders.

Except construction of brain template, we also provide generation of three different tissue templates including gray matter(GM), white matter(WM) and cerebral spinal fluid(CSF). All images are segmented in advance and then transformed to template space resulting the tissue templates.

In order to obtain the information of Talairach coordinates, we also provide a tool to derive the Talairach coordinates from our template space.

1.4 Thesis Organization

In the following chapters, we will present our algorithms, experiment results, discussion and conclusion. In chapter 2, we bring up our idea of automatic procedure of template construction. Because we try to verify the constructed templates, in chapter 3, we make a description of the template evaluation metrics. In chapter 4, we show all the experiment results. Then we have a discussion about the experiment results in chapter 5. Finally, in chapter 6, we make a conclusion.

Chapter 2

Template Construction Method



2.1 Introduction

The process of automatically constructing a spatially unbiased template can be described in following steps, which is depicted in Fig. 2.1.

1. Nonuniformity correction
2. Selection of representative brain
3. Determination of unbiased stereotaxic space
4. Transformation and averaging



First, we use Non-parametric Non-uniform intensity Normalization (N3) [26] technique, provided by Montreal Neurological Institute, to correct the nonuniformity of image. In the following steps, we use the corrected images to be processed. Second, because every brain images should be registered to a stereotaxic space before calculating the unbiased space, a reference brain is needed. We choose a brain volume, which is one subject of the image set and has the minimum variation of deformation magnitude to the other subjects, as the representative brain. Then we will define the unbiased space based on this representative brain. Thirdly, we compute the unbiased space according to the representative brain and all other brain images. Finally, we normalize all images to the unbiased space and average them to generate the brain template.

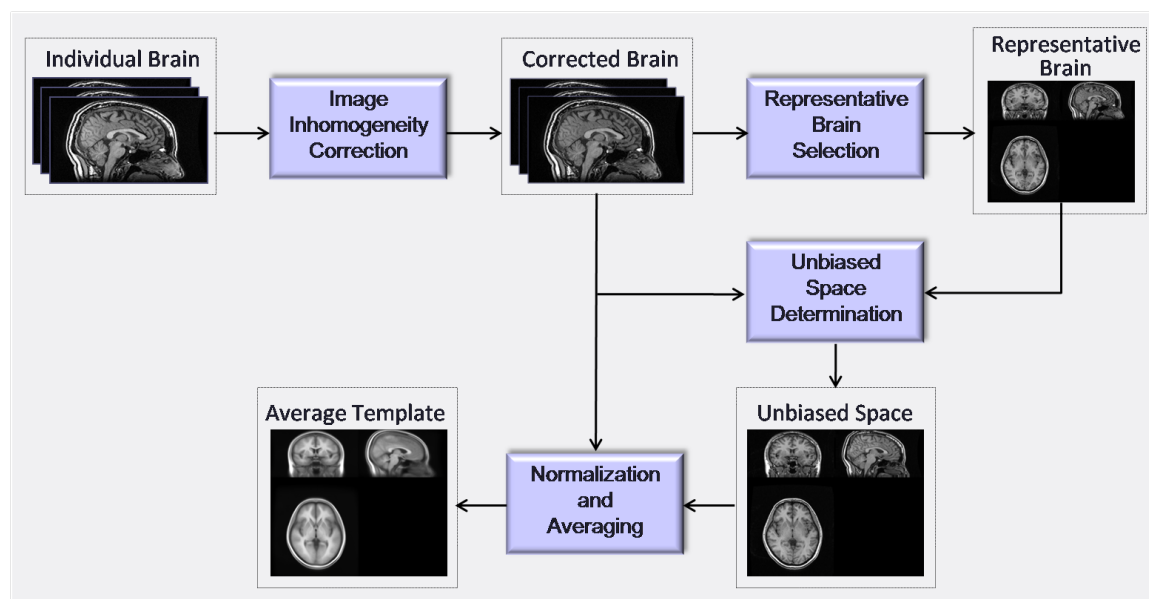


Figure 2.1: **Flow chart of template construction.** This figure describes the processed flow chart of the template construction. First, nonuniformity correction is performed to acquire images with better qualities. Second, a representative brain is selected among the data set to serve as the reference volume. Thirdly, the unbiased space is determined based on the selected representative brain and all other images. Finally, all images are transformed to this unbiased space and averaged to become the brain template.

2.2 Nonuniformity Correction

An intensity artifact, which the signal intensity vary smoothly across an image, is often seen in MR images. Various referred to radio frequency (RF) inhomogeneity, shading artifact, or intensity non-uniformity, it is usually attributed to poor RF field uniformity. However, the image nonuniformity may significantly degrade the performance of automatic segmentation and interfere in quantitative analysis. Therefore, the removal of intensity nonuniformity (“bias”) from MRI images is an essential prerequisite for the quantitative analysis of MRI brain volumes. Fig. 2.2 shows the nonuniformity of MR images of a subject in our database.

Non-parametric Non-uniform intensity Normalization (N3) [26] technique have been

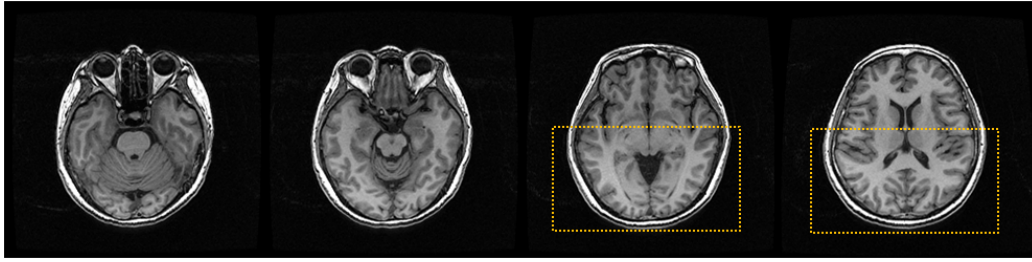


Figure 2.2: **Nonuniformity of MR images.** This figure shows the nonuniformity of MR images of a subject. There are four different slices in axial view of an individual brain. We can see the nonuniformity appeared, which the posterior white matter (in yellow region) is lighter than the anterior white matter.

devised in order to correct this intensity nonuniformity without requiring supervision. Without anatomy model assumptions, an iterative approach is employed to estimate both the multiplicative bias field and the distribution of the true tissue intensity in N3 method. It models the low-frequency spatial variations in the data to maximize high-frequency information in the intensity histogram of the corrected volume. The N3 algorithm was demonstrated a high degree of stability [2], represents an elaboration of tissue signal analysis. Also N3 substantially improve the accuracy of anatomical analysis techniques such as tissue classification, cortical surface extraction [26] and grey matter segmentation for voxel-based morphometry [1]. An executable version of the N3 algorithm was provided by Dr. A. C. Evans at the Montreal Neurological Institute, and program default values were used for all run-time parameters.

2.3 Image Registration

Registration of structural brain images typically include affine transformation and non-linear deformation. In general, affine transformation, or called global normalization, is composed of zero or more linear transformations, including translation, rotation, scaling and shearing. Further, nonlinear deformation is used to match the subject to the target im-

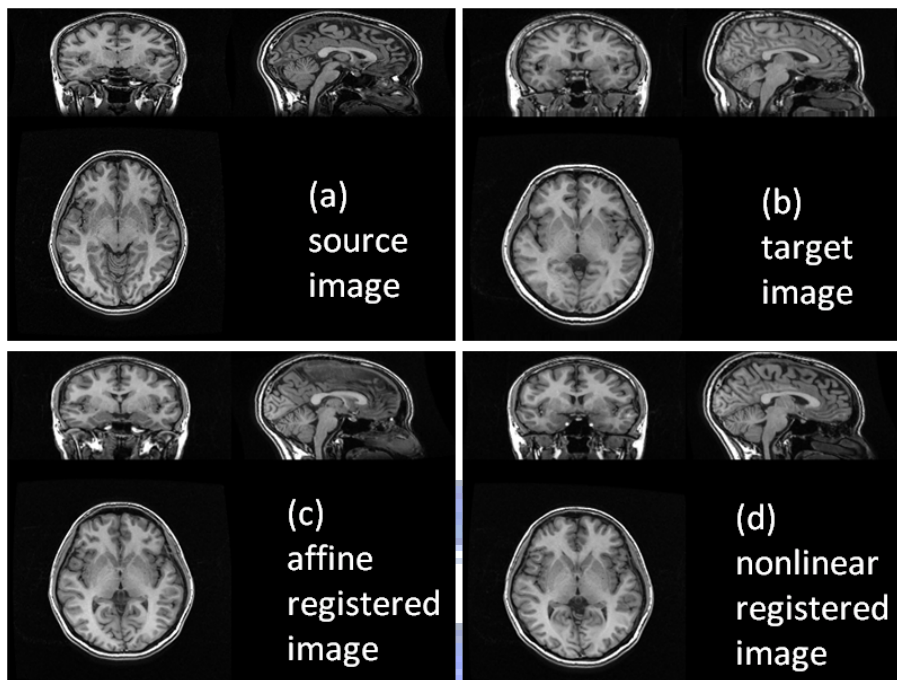


Figure 2.3: **Affine registration and nonlinear registration.** This figure shows the affine registration and nonlinear registration results. (a) This is the source image which is normalized to the target image. (b) This is the target image. We can tell the different brain size and shape between the source and the target. (c) The affine registered image of the source image is presented. The source image now is roughly registered to the target with the brain size. (d) The nonlinear registered image of the source image is showed. We can see the anatomical structure of the source brain is now registered to the target image, especially the corpus callosum region.

age on a regional level. The registration method adopted in this study is proposed by Liu et al. [18]. In their study, simulation data were used for validations and experiment results showed that the proposed registration approaches can efficiently register brain images with high accuracy compared to other algorithms, such as SPM2, AIR5 and ART. Fig. 2.3 shows the affine registration and nonlinear registration results of a subject in our database.

In image registration, two images are performed by serious deformations in order to make one image identical to the other. The result is stored in a deformation field, a vector field which records the magnitude and direction required to deform a point in the source

image to the appropriate point in the target image. The deformation function is

$$x_T = x_S + \mathbf{d}_{ST}(x_S) \quad (2.1)$$

, which x_T is a point in the target image, x_S is a point in the source image and $\mathbf{d}_{ST}(x_S)$ is the deformation vector of the point x .

2.4 Selection of Representative Brain

Because every brain images should be registered to a stereotaxic space before calculating the unbiased space, a reference brain is needed [16]. There are several choices to select a reference volume such as the MNI305 template and the ICBM152 template. However, these different ethnic templates may cause large deformation while registering Taiwanese subject to them. Large deformation often conduct inaccuracy or instability of registration. Thus, we choose a brain volume, which is one subject of the image set and has the minimum variation of deformation magnitude to the other subjects, as the representative brain. In other words, the representative brain is defined to be the brain that is closer to all the brains than others. The definition of representative brain is as follows:

$$R = \arg \min_j \{var(\|\mathbf{d}_{ij}(x_i)\|)\}, \quad \forall j \neq i, x_i \in \text{brain area}, \quad (2.2)$$

where $\mathbf{d}_{ij}(x_i)$ is the deformation vector from subject i to subject j at position x_i in the space of subject i . The subject which has the minimum cost function, variation of deformation magnitude, with all the other subjects is chose as representative brain R . We describe this idea in Fig. 2.4.

2.5 Determination of Unbiased Stereotaxic Space

Our goal is to create an unbiased space, the template, in which the structure location at the template denoted as x_T should be equal to the expected location of that structure loca-

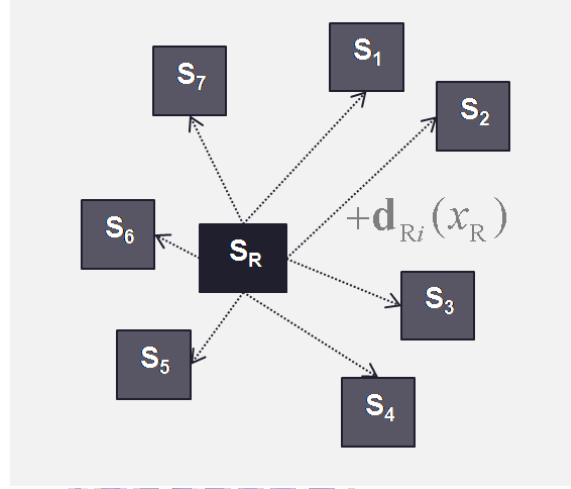


Figure 2.4: **The sketch map of selection of the representative brain.** Suppose there are eight subjects in the data set, S_1, S_2, \dots, S_7 and S_R . When we register S_R to other seven subjects, we will obtain seven deformation fields $\mathbf{d}_{Ri}(x_R)$, which $i = 1, 2, \dots, 7$. S_R will be the selected representative brain if it has the minimum value of $\text{var}(\|\mathbf{d}_{Ri}(x_R)\|)$ compared with other subjects.

tion at subject i , denoted as x_i , across all individuals N (a similar argument in Diedrichsen J. et al. [8]) [12] [14]:

$$x_T = E\{x_i\}, \quad (2.3)$$

where $i = 1, 2, \dots, N$. That is, the expected deformation vector between x_T and x_i is zero. However, we can regist representative brain R to subject i to get the deformation field. Referring to equation 2.1, $\mathbf{d}_{Ri}(x_R)$ is the deformation vector from representative brain R to subject i at position x_R . Thus,

$$x_i = x_R + \mathbf{d}_{Ri}(x_R), \quad (2.4)$$

which $x_R + \mathbf{d}_{Ri}(x_R)$ is the location in the space of subject i . Trivially,

$$E\{x_i\} = E\{x_R + \mathbf{d}_{Ri}(x_R)\} = x_R + \bar{\mathbf{d}}_R(x_R), \quad (2.5)$$

where $\bar{\mathbf{d}}_R$ is the average deformation field which calculated by

$$\bar{\mathbf{d}}_R(x_R) = \frac{1}{N} \sum_{i=1}^N \mathbf{d}_R(x_R). \quad (2.6)$$

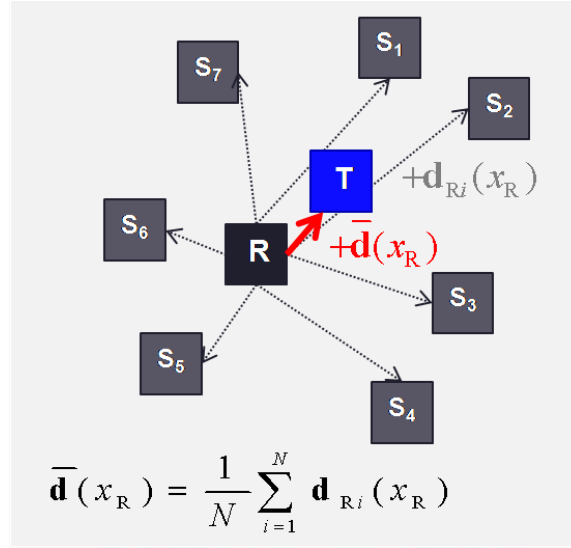


Figure 2.5: **The sketch map of transforming representative brain to the unbiased space.** Suppose there are eight subjects in the data set, S_1, S_2, \dots, S_7 and R . When we register representative brain R to other seven subjects, we will obtain seven deformation fields $\mathbf{d}_{Ri}(x_R)$, which $i = 1, 2, \dots, 7$. Then we use the equation 2.6 to derive the average deformation field $\bar{\mathbf{d}}_R$. By applying the average deformation field $\bar{\mathbf{d}}_R$ to the representative brain R to result the unbiased template space T .

Therefore, referring to equation 2.3 and equation 2.5, the template space can be defined as

$$x_T = x_R + \bar{\mathbf{d}}_R(x_R), \quad (2.7)$$

which means that applying the average deformation field to the representative brain R to result the unbiased template space T . We describe this notation in Fig. 2.5.

The representative brain is registered to each nonuniformity-corrected image. We obtain each deformation field $\mathbf{d}_{Ri}(x_R)$ and average them to become the average deformation field $\bar{\mathbf{d}}_R$. It is notable that the deformation vectors, stored in the average deformation field, record the vector required to deform points, called voxels, in representative brain to the appropriate voxels in unbiased space. This unbiased space is our template space.

However, due to the sub-voxel accuracy of the average deformation field $\bar{\mathbf{d}}_R$, the intensity of each voxel x_T is not trivially known. We illustrate the concept with Fig. 2.6.

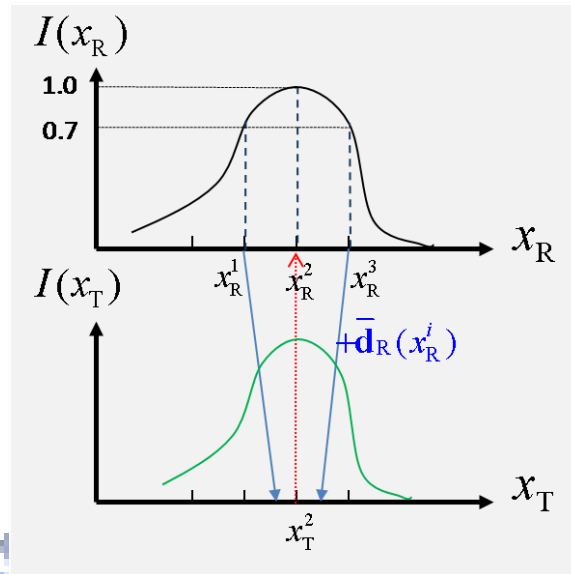


Figure 2.6: **The sketch map of interpolating the mapping coordinate in the unbiased space.** The intensity profile of the representative brain is shown as $I(x_R)$. When compressing the profile of representative to become the profile of the template, the ideal profile of template is shown as $I(x_T)$ (green profile). x_R^1 and x_R^3 plus the average deformation vectors, $\bar{d}_R(x_R^1)$ and $\bar{d}_R(x_R^3)$ to the sub-voxel position in unbiased space. However, the intensity of x_T^2 must not be derived by simply averaging the intensity of $I(x_R^1)$ and $I(x_R^2)$, which is 0.7. Instead of averaging the intensity, it should calculate the corresponding position in the x_R , which is x_R^2 in this case, and finally derive the intensity of x_T^2 , which is 1.0.

Suppose the image signal is a one dimensional signal, and the intensity profile of the representative brain is shown as $I(x_R)$. The point x_R^1 and x_R^3 are deformed to sub-point position in template space. In that case, the intensity of point x_T^2 in template space is not to know. However, the intensity of x_T^2 must not be derived by simply averaging the intensity of $I(x_R^1)$ and $I(x_R^2)$. Instead of averaging the intensity, it should calculate the corresponding position in the x_R , which is x_R^2 in this case, and finally derive the intensity of x_T^2 .

In this thesis, we propose a interpolation method to calculate the corresponding position in the x_R . A voxel x_T in the unbiased space, or said template space, is corresponding to x_R^T in the representative space. Then the intensity of x_T is $I(x_T)$ is defined as:

$$I(x_T) = I(x_R^T). \quad (2.8)$$

We interpolate the x_R^T position by the following equation :

$$x_R^T = \frac{1}{\sum_{i=1}^{M_T} w_i} \sum_{i=1}^{M_T} w_i y_i, \quad y_i \in \text{neighbor of } x_T. \quad (2.9)$$

In equation 2.9, w is the Gaussian weight which defined as

$$f(x, y, z) = A e^{-\left(\frac{(x-x_0)^2}{2\sigma_x^2}\right) - \left(\frac{(y-y_0)^2}{2\sigma_y^2}\right) - \left(\frac{(z-z_0)^2}{2\sigma_z^2}\right)},$$

which $f(x, y, z)$ is the Gaussian value according the center at (x_0, y_0, z_0) , A is the Gaussian amplitude, and $\sigma_x, \sigma_y, \sigma_z$ are the the x, y and z spreads of the blob. Therefore, by equation 2.8 and equation 2.9, we finally derive the intensity of all voxels in the unbiased space.

2.6 Average Template in Unbiased Space

After we derive the unbiased space, we normalize all MR T1-images, which have been corrected the intensity inhomogeneity, to the unbiased space. Then we average them to become the average template. However, because this unbiased space is derived from the representative brain, the brain size and orientation of the generated template is significantly dependent on the representative brain. Suppose the representative brain is not located in the center of the MR image, then the brain template will not located in the center of the MR image. Fig. 2.7 describes the processed flow chart of the average template.

2.7 Brain Tissue Templates

Brain tissue could be classified into three different types, gray matter (GM), white matter (WM) and cerebral spinal fluid (CSF). In the thesis, GM, WM and CSG tissue templates are generated by the following steps:

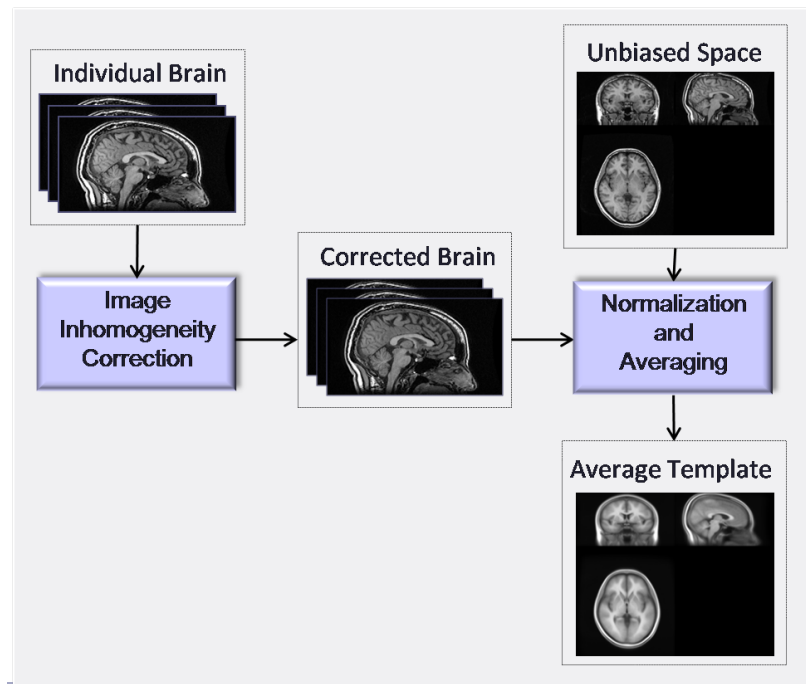


Figure 2.7: **Flow chart of average template construction.** This figure describes the processed flow chart of the average template. The average template in unbiased space is constructed by normalizing all individual images to the unbiased space then averaging them to become the average unbiased template.

- (1) Segment each individual brain into three tissue classes (GM, WM and CSF).
- (2) Register each T1-weighted image to the unbiased template and obtain its deformation field.
- (3) Normalize every tissue segment of all individuals by their own deformation field in step 2.
- (4) Average all these normalized tissue segments and finally form the templates of three tissue classes.

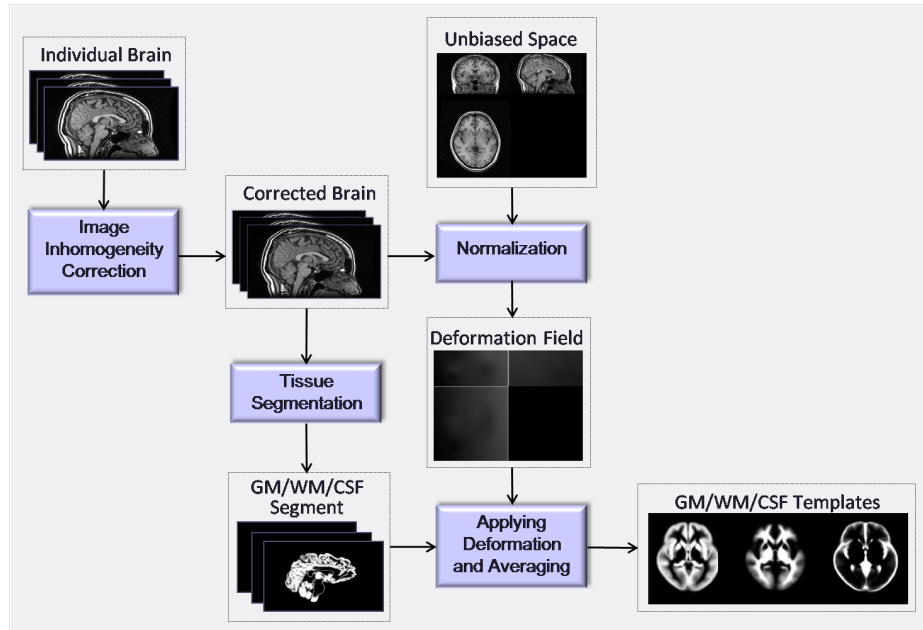


Figure 2.8: **Flow chart of tissue templates construction.** This figure describes the processed flow chart of the tissue templates. First, we segment each individual brain into GM, WM and CSF by FMRIB's Automated Segmentation Tool (FAST). Then we register each T1-weighted image to the unbiased template and obtain its deformation field. After we obtain the deformation field, we normalize every tissue segment of each individual by applying its own deformation field. Finally, the tissue templates are generated by averaging all these normalized tissue segments.

Segmentation are performed by FMRIB's Automated Segmentation Tool (FAST) [27] [13]. The tissue templates procedure is shown in Fig. 2.8.

2.8 Mapping to Talairach Coordinate System

Talairach coordinate system is widely used as a reference with Brodmann cytoarchitectonic areas and other structural and functional labels. Therefore, we should provide the mapping method between our template and the Talairach coordinate system. In other words, we intend to create a transformation to apply to the coordinates from the our brain template, to give matching coordinates in the TB. However, because there is no MRI scan

for the Talairach brain, we are incapable of using computerized registration to simply transform our template to Talairach brain.

Since there are already tools that can transform a coordinate in the MNI template space to the Talairach space [6], we use MNI template as the bridge to Talairach space by transforming the coordinate in our template to MNI template first. Thus, the mapping coordinate in Talairach space will be calculated by the second transformation from MNI305 to Talairach space.

To implement the method illustrated above is registering our template to the MNI template to obtain the deformation field. This deformation field stores the appropriate mapping coordinate in MNI template space of every voxel in our template. Then we derive Talairach coordinates from `mnit2tal` script (<http://www.mrc-cbu.cam.ac.uk/~matthew/abstracts/MNI-Tal/mnital.html>), a tool commonly used to map MNI coordinates to Talairach coordinates [3]. Also we register MNI template to our template and transform the coordinate in Talairach space to our template space.





Chapter 3

Template Evaluation Method



3.1 Introduction

In order to quantitatively evaluate the constructed template in comparison with the different templates, including the widely-used template nowadays, we use two metrics in our evaluation procedure. The template serves as the reference space for all images transforming to it. Thus, the template, which provides the better registration accuracy for all images of the study group, can be defined as the better template. Therefore, we use two metrics to verify the performance that our template improves. The two factors are:

1. Nonlinear deformation field between subjects and templates
2. Similarity between registered subjects and templates

3.2 Nonlinear Deformation Field between Subjects and Templates

3.2.1 Magnitude of Deformation Field

A good template should cause distortion of deformation as small as possible because large deformation may raise registration inaccuracy. Therefore, magnitude of deformation field is a good way to measure the distortion. This evaluation aims to study the amount of local nonlinear deformation needed to perform the normalization. A small total amount of these local changes indicates a small overall difference in shape between images and template [15].

After normalizing every individual brain to a brain template, the nonlinear deformation

field can be calculated as the distance between corresponding points in the template and the original image after affine transformation. We average the magnitude of nonlinear deformation vectors for overall voxels of each individual brain. The magnitude of nonlinear deformation field is defined as average distance (AD):

$$AD = \frac{1}{MN} \sum_{i=1}^N \sum_{x=1}^M \mathbf{d}_{Ti}(x_T), \quad \forall x_T \in \text{brain area of the template}, \quad (3.1)$$

which M is the total number of voxels in brain area.

However, in order to examine the distribution of average nonlinear deformation magnitude, we also display the topography of deformation. While calculating the deformation field from the template to individual brains, magnitude of nonlinear deformation field on same voxel of every brain were recorded. Then we calculate the mean of the recorded values for every voxel. Thus, we can investigate the distribution of nonlinear deformation magnitude.

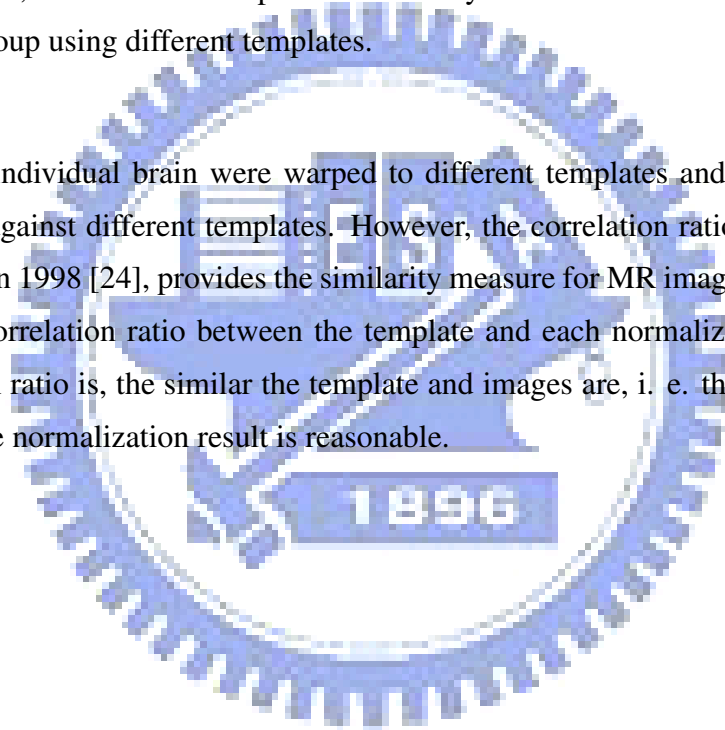
3.2.2 Variance of Deformation Field

By observing the variance of nonlinear deformation field, we can know the anatomically regional variability of the difference between the template and individual brains. However, a good template should cause not only small distortion magnitude of deformation but also small distortion variance. When the variance of nonlinear deformation field is zero, this template is called unbiased to the individual brains. For calculating the variance, when we normalize subjects to the template, the deformation magnitude of each voxel is recorded. We calculate the variance of all magnitudes in the same voxel of all brain images. Finally, we obtain the topography of variance of nonlinear deformation field.

3.3 Similarity between Registered Subjects and Templates

The deformation magnitude only provides the amount of normalization distortion. However, the less distortion can not imply the higher registration accuracy. That is to say, if we normalize a brain to a template which barely provides any information, the deformation is small but the result of registration is poor. For this reason, we aim to study the similarity between the template and the images after normalization for the anatomical evaluation. We anticipate that when using the better template, the warped brain images are more similar to the template. Here, we intend to compare the accuracy of normalization of all images of a study-specific group using different templates.

Each of the individual brain were warped to different templates and compared their spatial likeness against different templates. However, the correlation ratio, introduced by Roche, A. et al. in 1998 [24], provides the similarity measure for MR images. We calculate the average of correlation ratio between the template and each normalized images. The larger correlation ratio is, the similar the template and images are, i. e. the similar are the two, provided the normalization result is reasonable.



Chapter 4

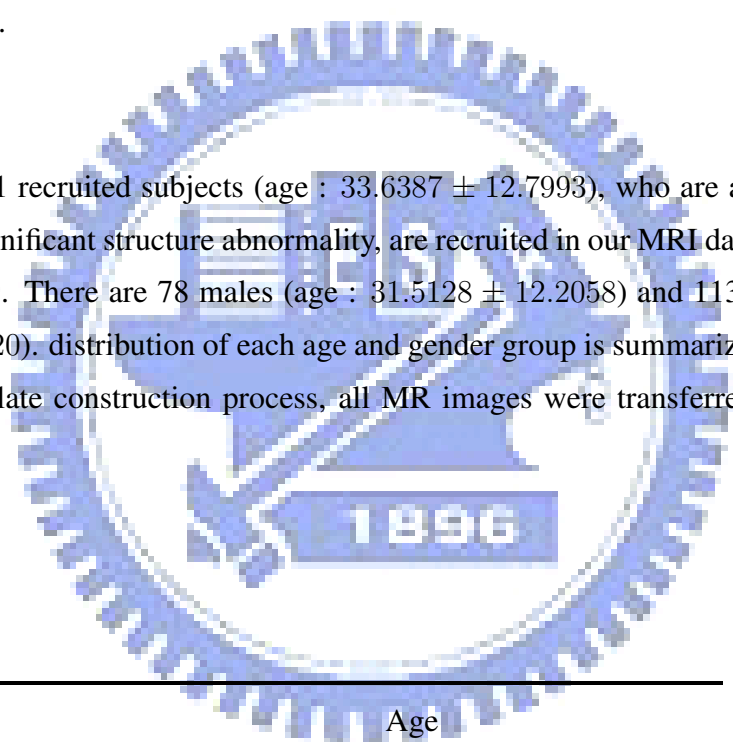
Experiment Results



4.1 Materials

The database was constructed with normal brains of different generations and genders. The magnetic resonance images were acquired on a 1.5 Tesla GE MR scanner, using 3D-FSPGR pulse sequence (TR = 8.67 ms, TE = 1.86 ms, TI = 400 ms, NEX = 1, flip angle = 15° , bandwidth = 15.63 kHz, matrix size = $256 \times 256 \times 124$, voxel size = $1.02 \times 1.02 \times 1.5$). All MR scans were collected by Integrated Brain Research Unit (IBRU) of Taipei Veterans General Hospital.

There are 191 recruited subjects (age : 33.6387 ± 12.7993), who are all right-handed and shown no significant structure abnormality, are recruited in our MRI database. The age range is 18 to 69. There are 78 males (age : 31.5128 ± 12.2058) and 113 females (age : 34.9464 ± 12.9920). distribution of each age and gender group is summarized in Table 4.1. Before our template construction process, all MR images were transferred into Analyze format.



	Age					
	18-19	20-29	30-39	40-49	50-59	60-69
Male	5	45	9	8	11	0
Female	14	34	29	13	19	4

Table 4.1: **Number of subjects in our database.**

4.2 Construction of Brain Templates

4.2.1 Nonuniformity Correction

We used Non-parametric Non-uniform intensity Normalization (N3) [26] tool to correct the nonuniformity of MR images in order to obtain the higher quality of images. An executable version of the N3 algorithm was provided by Dr. A. C. Evans at the Montreal Neurological Institute, and program default values were used for all run-time parameters. On the other hand, we used the nonuniformity correction tool provided by SPM2 to compare the performance with N3.

We examined the MR images which corrected by N3 tool and found N3 provide a high degree of stability and substantially improve the quality of the MR images. Here we randomly selected four subjects to show the results of nonuniformity correction in Fi. 4.1 and Fig. 4.2. In the subject1 and subject2, the nonuniformity of raw images are more evident than that in subject3 and subject4. However, the overall performance of N3 is better than SPM.

4.2.2 Selection of Representative Brain

Large deformation often conduct inaccuracy or instability of registration. Thus, we choose a brain volume, which is one subject of the image set and has the minimum variation of deformation magnitude to the other subjects, as the representative brain. Referring to equation 2.2, the $var(\|\mathbf{d}_{ij}(x_i)\|, \forall j \neq i)$ must be calculated. Take notice of $\|\mathbf{d}_{ij}(x_i)\|$ is not identical to $\|\mathbf{d}_{ji}(x_j)\|$. In other words, if we try to determine the representative brain within N subjects, we need to do the all-paired registration N^2 times.

In order to remove the aging problem of elder subject, we only recruited the subjects,

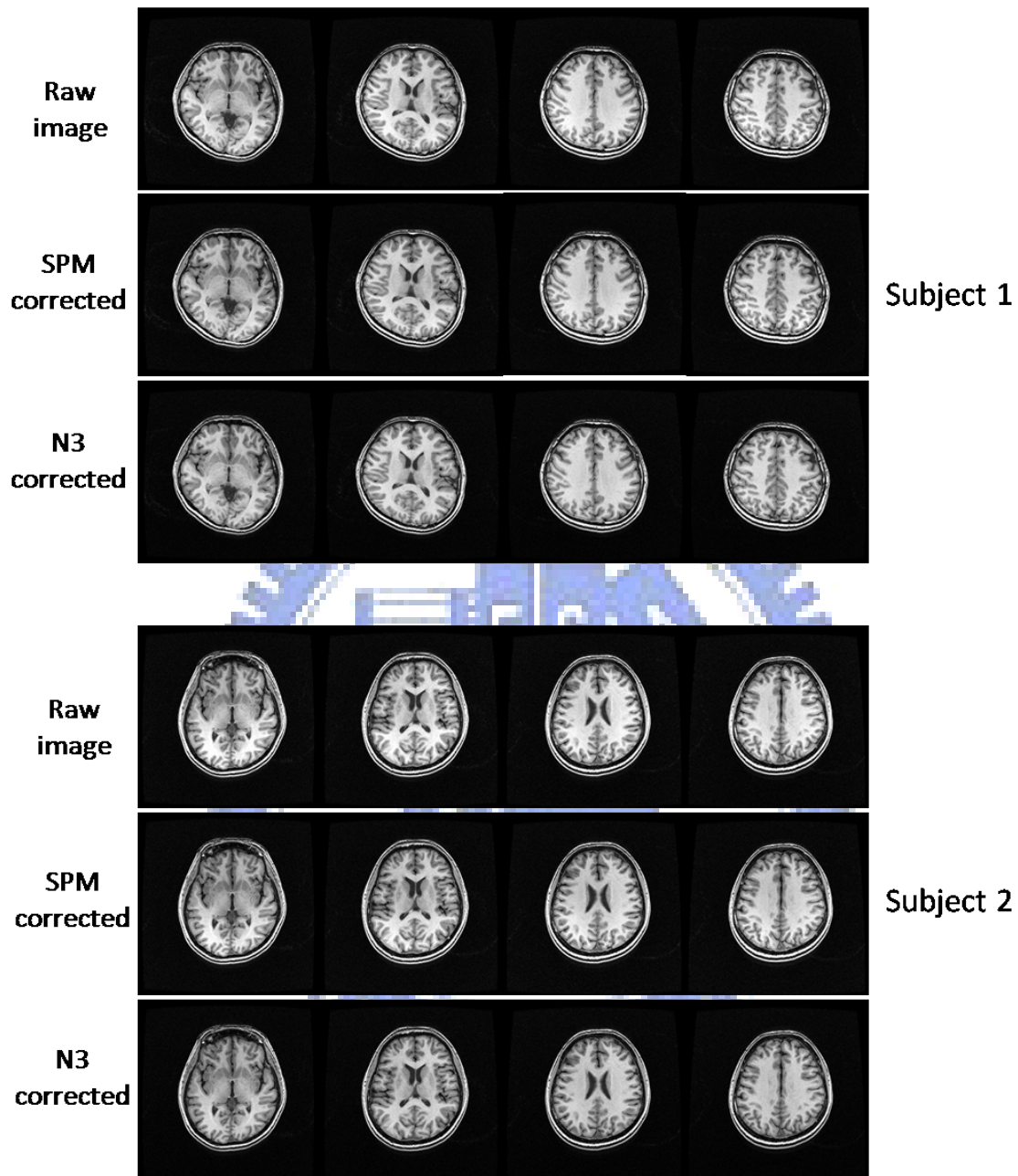


Figure 4.1: **Results of nonuniformity correction using SPM and N3 for subject1 and subject2.** For each subject, we showed four slices the raw image, nonuniformity correction using SPM and nonuniformity correction using N3 in three rows. We can see the nonuniformity appeared in raw the image, where the posterior region of white matter is lighter than the anterior white matter. The nonuniformity has been evidently improved after N3-correction comparing with SPM.

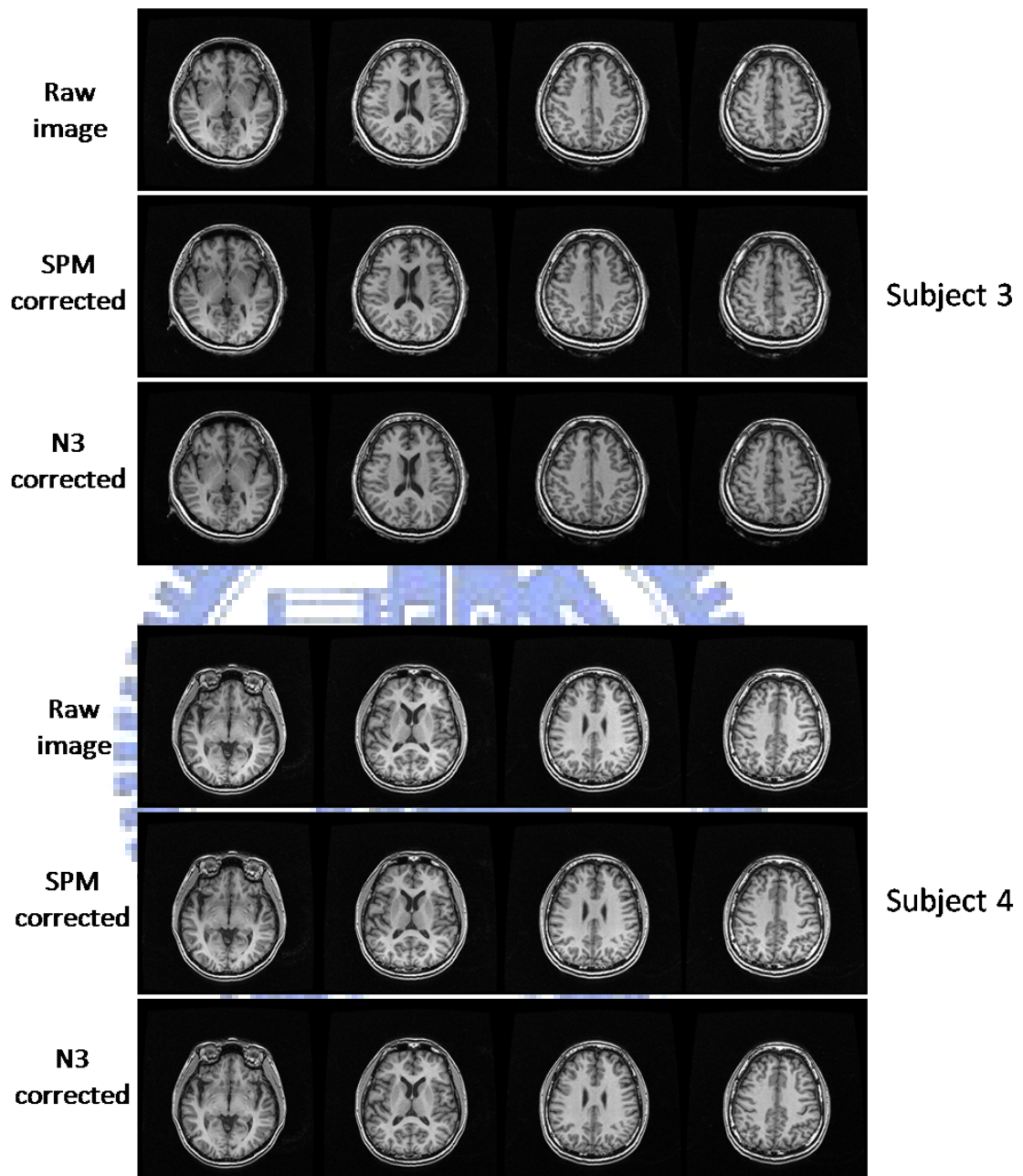
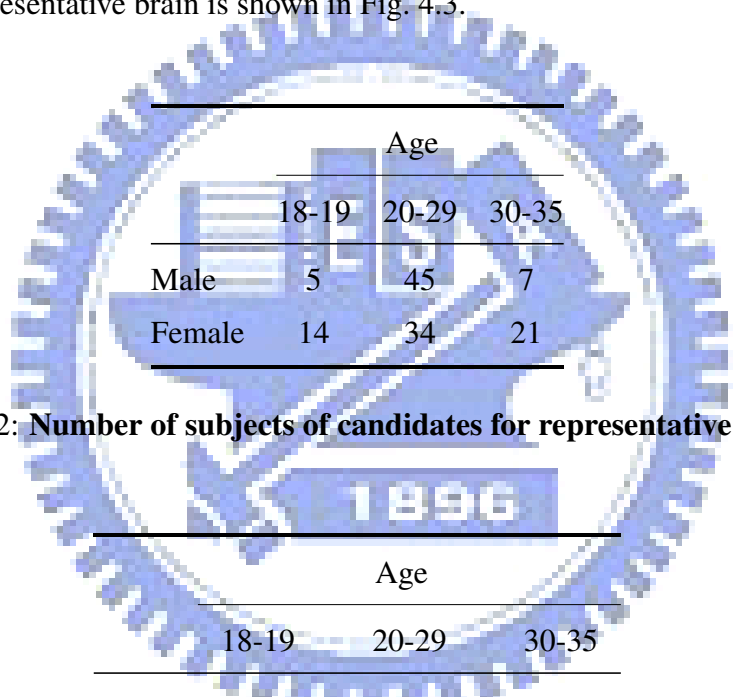


Figure 4.2: **Results of nonuniformity correction using SPM and N3 for subject3 and subject4.** For each subject, we showed four slices the raw image, nonuniformity correction using SPM and nonuniformity correction using N3 in three rows. We can see the nonuniformity appeared in raw the image, where the posterior region of white matter is lighter than the anterior white matter. The nonuniformity has been improved after N3-correction comparing with SPM.

which age range is 18 to 35 years old (25.5339 ± 5.0728), as the candidates of the representative brain. There are total 126 subjects, including 57 males and 69 females. Table 4.2 shows the distribution of each age and gender group. The value of the cost function, $\text{var}(\|\mathbf{d}_{ij}(x_i)\|, \forall j \neq i)$, is 78.3439 ± 160.2550 mm/voxel. Table 4.3 lists the mean value of the cost function in each group.

A 23 years old female is selected as the representative brain within 126 subjects. It's value of cost function is 6.8458, which is the minimum value of all 126 subjects. The MR image of the representative brain is shown in Fig. 4.3.



	Age		
	18-19	20-29	30-35
Male	5	45	7
Female	14	34	21

Table 4.2: **Number of subjects of candidates for representative brain.**

	Age		
	18-19	20-29	30-35
Mean	74.1643	77.1644	84.5079
Std.	101.8881	145.4536	225.3896

Table 4.3: **Mean and standard deviation of cost function for selection of representative brain.**

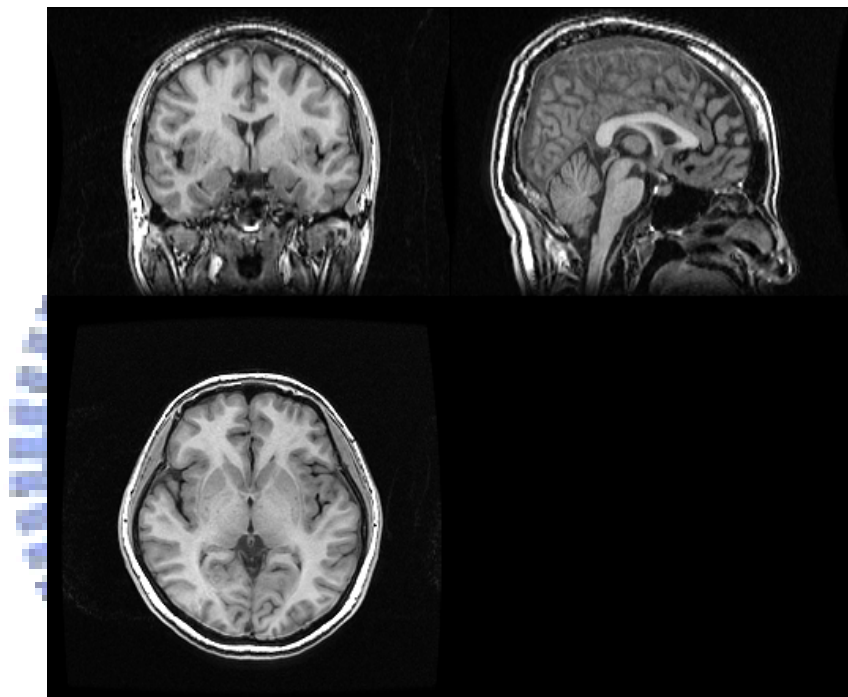


Figure 4.3: **The selected representative brain.** The selected representative brain, a 23 years old female's brain, from 126 subjects with age range from 18 to 35 years old.

4.2.3 Determination of Unbiased Stereotaxic Space

After selecting the representative brain, 191 normal subjects were taken to calculate the unbiased space. Age range is from 18 to 69 years old (33.6387 ± 12.7993). The representative brain was normalized to other 190 individual brains. We obtained the average deformation field by averaging all nonlinear deformation fields with respect to all 190 brains. Then we applied the average deformation field to the representative brain to derive the unbiased space. In this step, we utilized proposed interpolation method. Fig. 4.4 shows the representative brain and the derived unbiased space.

4.2.4 The Unbiased Average Templates

After we derived the unbiased space, we normalized all 191 MR T1-images in our database to the unbiased space. Then we averaged them to become the 191 average template. Otherwise, we segmented all 191 MR images into gray matter (GM), white matter (WM) and cerebral spinal fluid (CSF) and normalized them to this unbiased space according to their own deformation fields. GM, WM and CSF templates were also created. All these templates are shown in Fig. 4.5.

Prime Templat

We also constructed a brain template for the prime of life (Fig. 4.6(b)). There are 126 subjects, including 57 males and 69 female, which age range is 18 to 35 years old (25.5339 ± 5.0728). Number of subjects for construction is shown in Table 4.4. The representative brain for prime group is a 23-year-old female brain, which is identical to whole subject group.

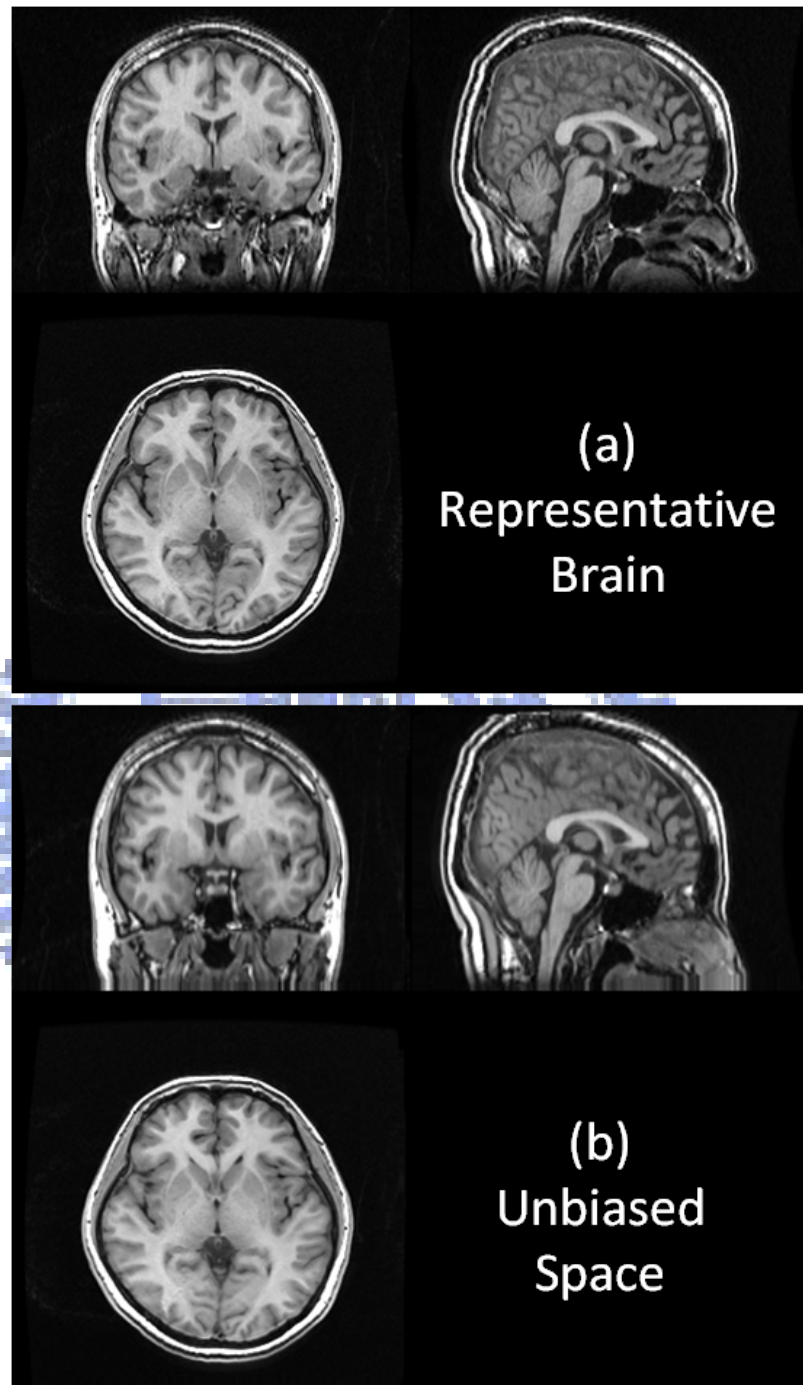


Figure 4.4: **The representative brain and the unbiased space.** (a) The representative brain. (b) The derived unbiased space from (a) and all other 190 subjects in MRI brain database.

Gender templates

We constructed brain template for both gender groups (Fig. 4.6(c)(d)). There are 57 males (age : 24.7895 ± 4.0565) and 69 female (age : 26.2754 ± 5.7596), which age range is 18 to 35 years old in our database. Number of subjects for construction is shown in Table 4.4. The representative brain for male group is a 24-year-old male brain. Additionally, the representative brain for female group is the same brain as for whole group, a 23-year-old female brain.

	Age		
	18-19	20-29	30-35
Male	5	45	7
Female	14	34	21

Table 4.4: Number of subjects for construction of prime template and gender template.

Age Templates

We constructed brain templates for each age groups, including 10 to 19, 20 to 29, 30 to 39, 40 to 49, 50 to 59 (Fig. 4.7). Table 4.1 shows number of data. However, because there are only 4 subjects that age range from 60 to 69 years old, there is no significance to build the template for this age group.

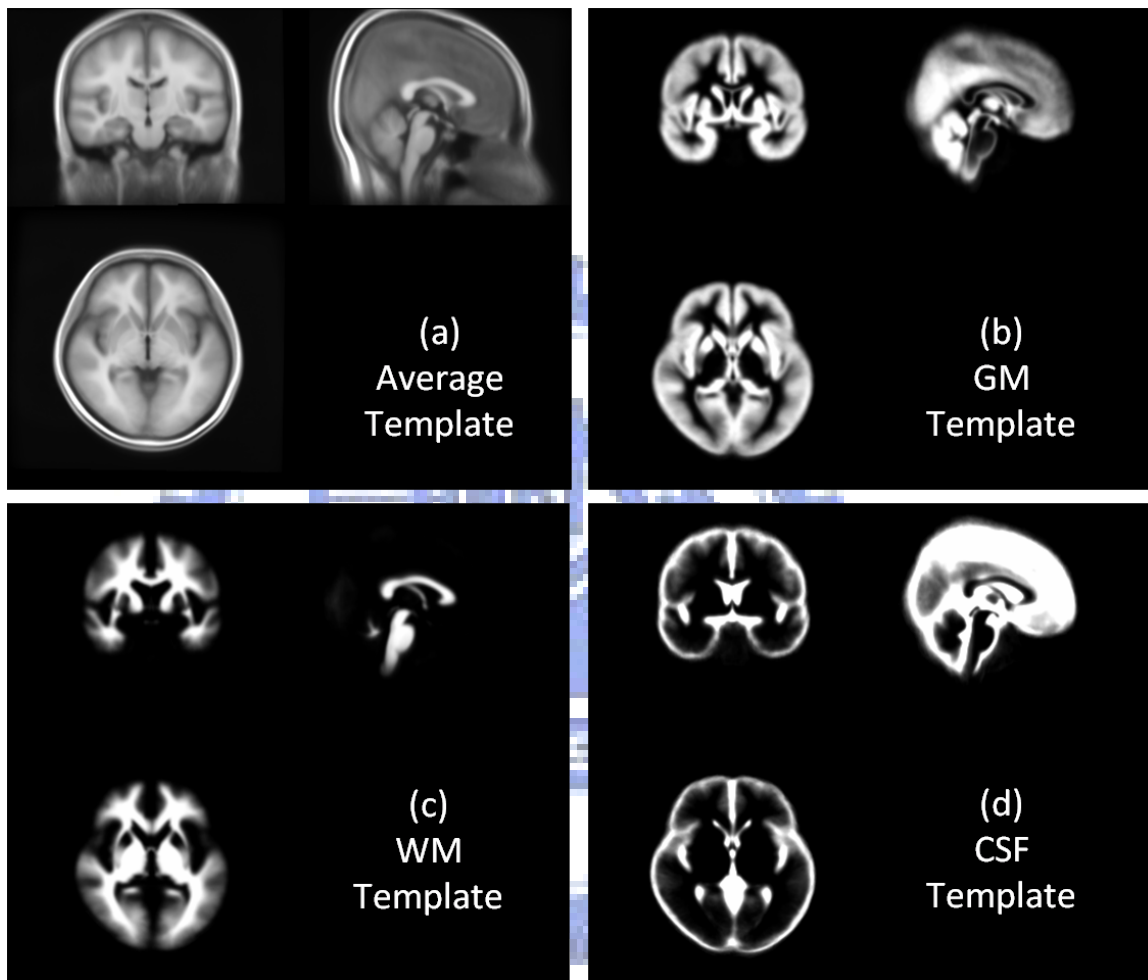


Figure 4.5: **The 191 average template and the tissue templates.** (a) The average template constructed from 191 subjects. (b) The GM template, (b) WM template and (c) CSF template.

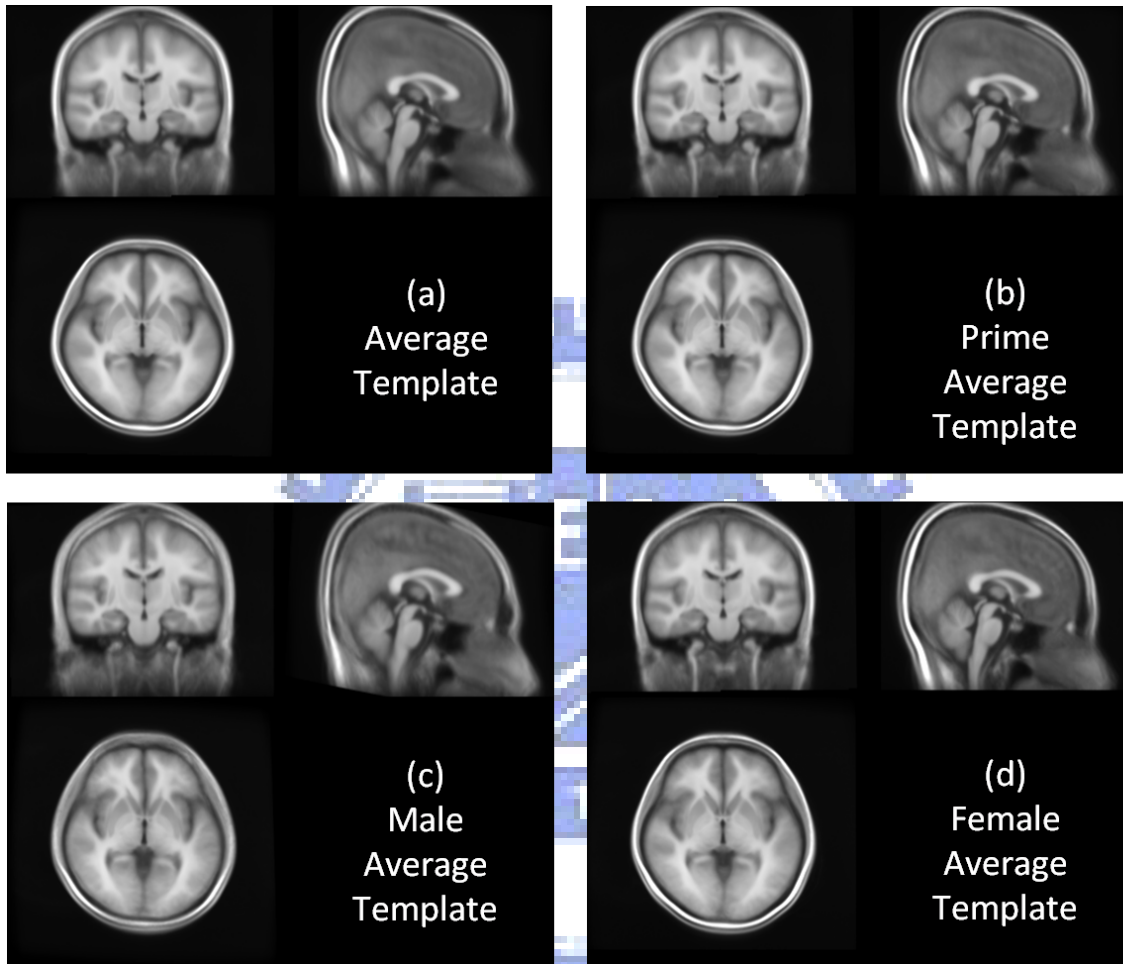


Figure 4.6: **The 191 average template, the prime template and the gender templates.** (a) The average template constructed from 191 subjects. (b) The prime template constructed from 126 subjects, which age range is from 18 to 35 years old. (c) The male template constructed from 57 male subjects (age : 24.7895 ± 4.0565). (d) The female template constructed from 69 female subjects (age : 26.2754 ± 5.7596). We affine registered these four templates together for the convenient and fair comparison.

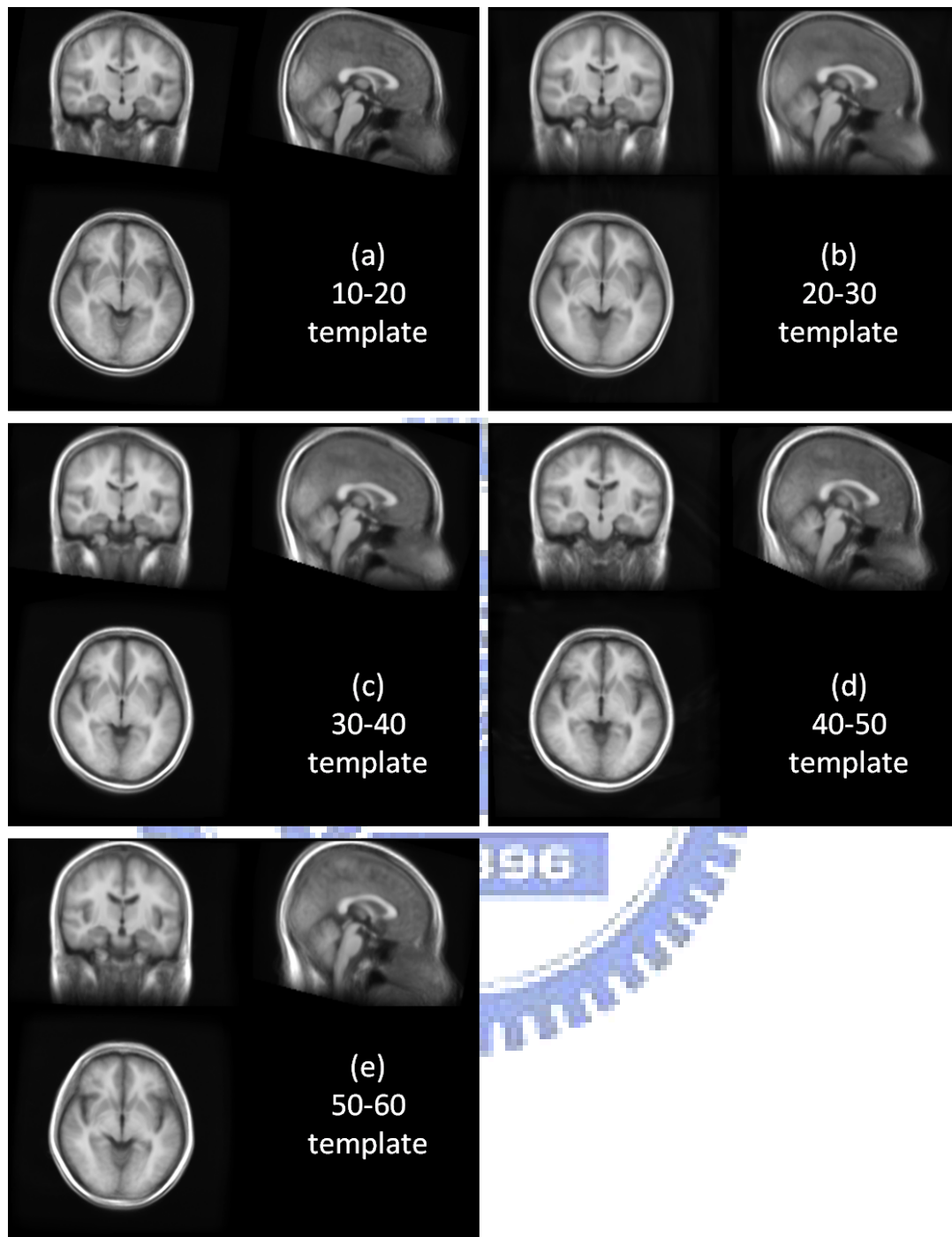


Figure 4.7: **The brain templates for each age groups.** (a) The template was constructed by subjects which from age 10 to 20. (b) The template was constructed by subjects which from age 20 to 30. (c) The template was constructed by subjects which from age 30 to 40. (d) The template was constructed by subjects which from age 40 to 50. (e) The template was constructed by subjects which from age 50 to 60. We affine registered these five templates together for the convenient and fair comparison.

4.3 Evaluation of Brain Templates

4.3.1 Nonlinear Deformation Field

When we normalized a MR brain images to a space, or a space, we obtained a deformation field. This evaluation aims to study the amount of local nonlinear deformation needed to perform the normalization.

Unbiased template v.s. ICBM152

We normalized all subjects, 191 subjects in our database, to the average template constructed from these 191 subjects and the ICBM152 template. The average magnitude of local nonlinear deformation of all subjects was listed in Table 4.5. We displayed the distribution of regional nonlinear deformation magnitude in brain region of each template (Fig. 4.8). While calculating the deformation field from each template to 191 individual brains, magnitude of nonlinear deformation field on same voxel of every brain were recorded. Then we calculated the mean of the recorded values for every voxel. Finally, a brain volume that its voxel value represents mean value of magnitude on same voxel was generated. Here we took the unbiased space, the unbiased average template generated by 191 subjects and ICBM152 to observe the regional magnitude of nonlinear deformation.

Otherwise, we also calculated the variance of deformation of these two templates (Fig. 4.9). We normalized all subjects, 191 subjects in our database, to two different templates, the average template created from these 191 subjects and the ICBM152 template. The deformation vector in each voxel was recorded in the 191 deformation field. Then we calculated the variance of the recorded values for every voxel. Finally, a brain volume that its voxel value represents the variance of deformation vector on same voxel was generated.

	Template	
	Unbiased average template	ICBM152
AD	1.7556	2.4572
Var.	7.6677	8.4774

Table 4.5: **The mean and variance magnitude of nonlinear deformation comparing Unbiased template v.s. ICBM152.** The mean and variance magnitude of nonlinear deformation from 191 subjects to both the unbiased template created from these 191 subjects and ICBM152 template were listed.

In order to evaluate the unbiased template with ICBM152 disinterestedly, we used 65 elder subjects, age range is from 36 to 69, in our database as the testing data. We normalized these 65 subjects to the prime-age template, which was constructed by 126 prime-age subjects, age range is from 18 to 35. In this case, the prime-age unbiased template was not consisted of any testing data. In the other hand, we also normalized these 65 subjects to ICBM152. We calculated the nonlinear deformation magnitude and variance from all 65 subjects to both templates. The mean of magnitude and variance is listed in Table. 4.6. We displayed the distribution of regional nonlinear deformation magnitude in brain region of each template (Fig. 4.10) and nonlinear deformation variance (Fig. 4.11).

	Template	
	Prime-age unbiased template	ICBM152
AD	0.8215	1.9907
Var.	4.1604	9.9779

Table 4.6: **The mean and variance magnitude of nonlinear deformation comparing prime-age unbiased template v.s. ICBM152.** The mean and variance magnitude of nonlinear deformation from 65 elder subjects to both the prime-age unbiased template created from prime-age 126 subjects and ICBM152 template were listed.

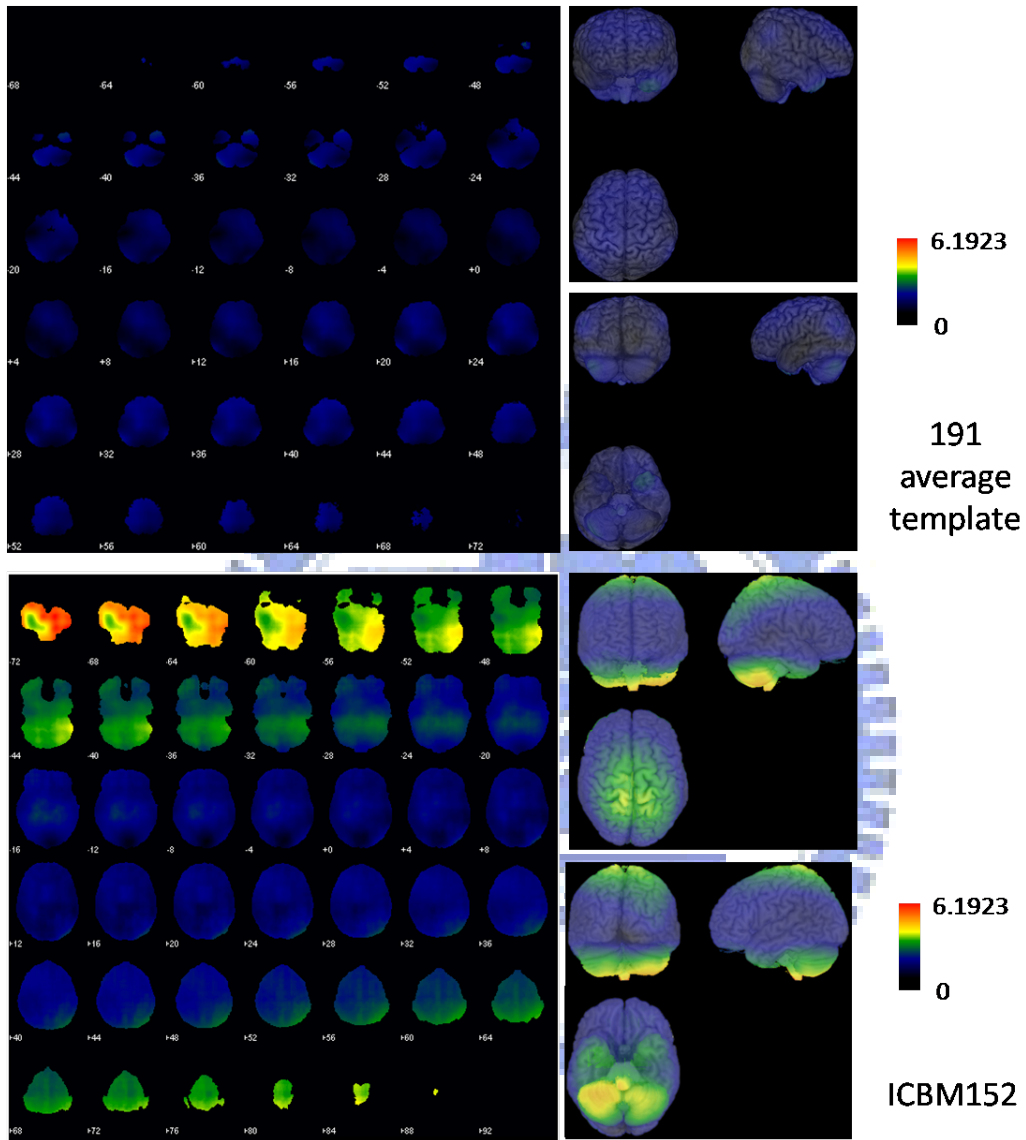


Figure 4.8: **The distribution of nonlinear deformation magnitude to Unbiased Template and ICBM152 template.** We normalized 191 brain images to both the unbiased template constructed by these 191 subjects and ICBM152 template. We averaged the magnitude of nonlinear deformation on the same voxel of each brain. Then, the brain volume that its voxel value represents the mean of the nonlinear deformation was formed. The left figure showed the distribution on slices in axial view.

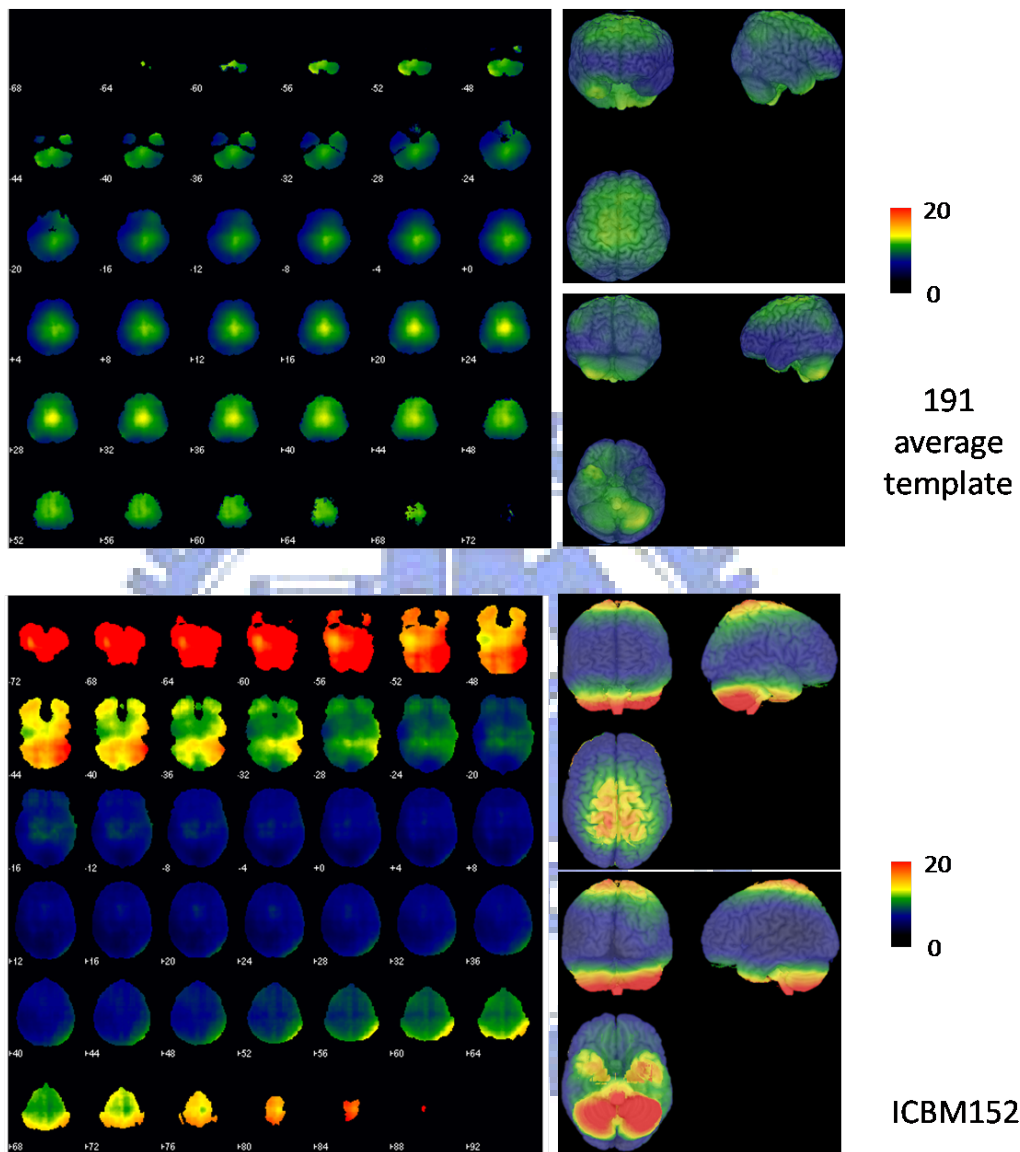


Figure 4.9: **The distribution of nonlinear deformation variance to Unbiased Template and ICBM152 template.** We normalized 191 brain images to both the unbiased template constructed by these 191 subjects and ICBM152 template. We calculated the variance of nonlinear deformation on the same voxel of each brain. Then, the brain volume that its voxel value represents the variance of the nonlinear deformation was formed. The left figure showed the distribution on slices in axial view.

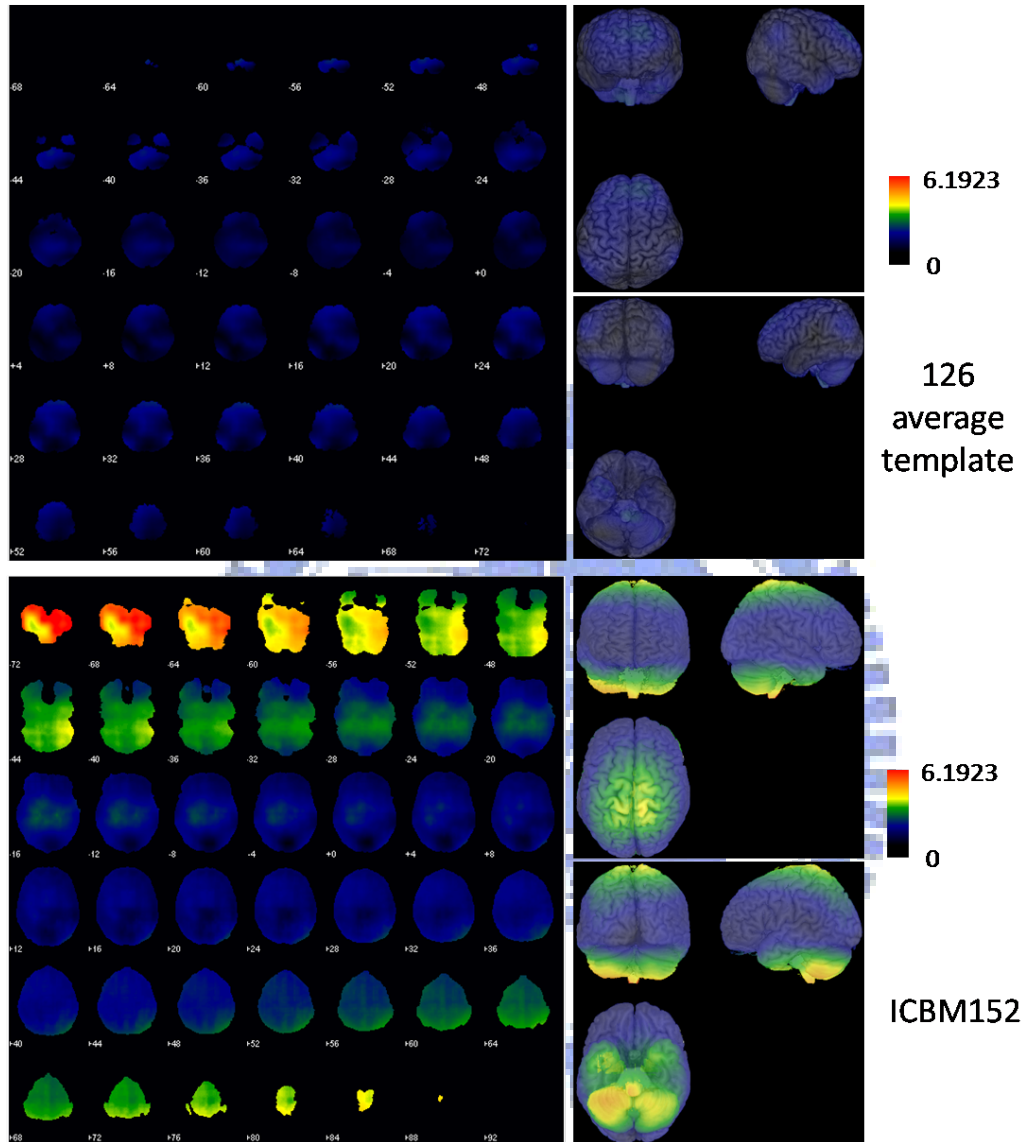


Figure 4.10: **Nonlinear deformation magnitude of 65 elder subjects to prime-age unbiased template and ICBM152 template.** We normalized 65 elder brain images to both the prime-age unbiased template constructed by 126 prime-age subjects and ICBM152 template. We averaged the magnitude of nonlinear deformation on the same voxel of each brain. Then, the brain volume that its voxel value represents the mean of the nonlinear deformation was formed. The left figure showed the distribution on slices in axial view.

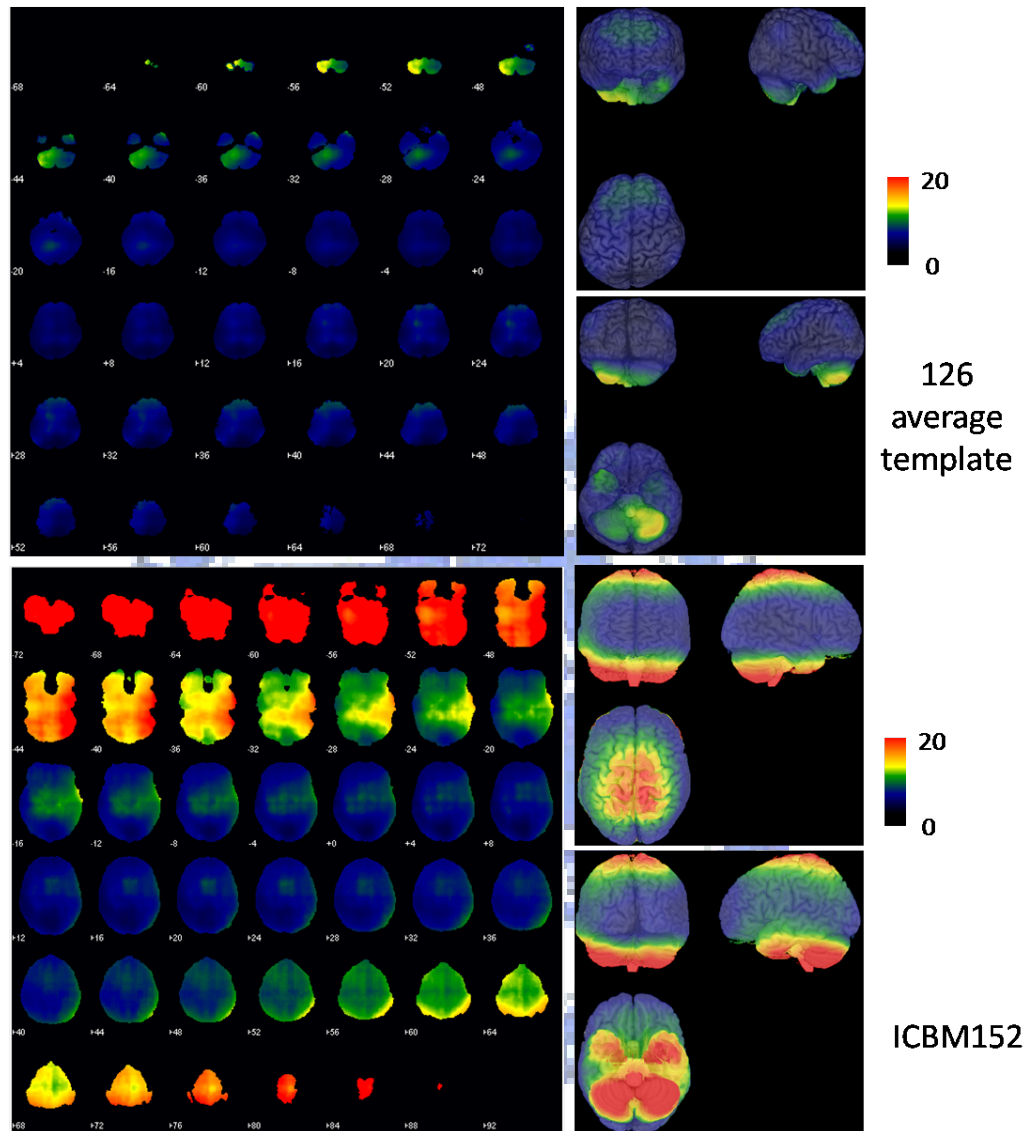


Figure 4.11: **Nonlinear deformation variance of 65 elder subjects to prime-age unbiased template and ICBM152 template.** We normalized 65 elder brain images to both the prime-age unbiased template constructed by 126 prime-age subjects and ICBM152 template. We calculated the variance of nonlinear deformation on the same voxel of each brain. Then, the brain volume that its voxel value represents the variance of the nonlinear deformation was formed. The left figure showed the distribution on slices in axial view.

Bisexual template v.s. gender template

We used proposed method in this thesis to construct the bisexual template, including 126 male and female subjects, and two gender templates, the male template constructed by 57 males and the female template constructed by 69 females. The subject number is in Table 4.7.

	Template		
	Bisexual template	Male template	Female template
Subjects	126	57	69
Age	25.5339 ± 5.0728	24.7895 ± 4.0565	26.2754 ± 5.7596

Table 4.7: **Number of subjects for construction of bisexual template and gender templates.**

We normalized 57 male subject brains to both the bisexual template and the male template and obtained the nonlinear deformation field. Also we normalized 69 female subject brains to both the bisexual template and the female template and obtained the nonlinear deformation field. The mean magnitude and variance of local nonlinear deformation of male and female subjects was listed in Table 4.8 and Table 4.9.

We displayed the distribution of regional nonlinear deformation magnitude or variance in brain region of both the bisexual template and gender template (Fig. 4.12 to Fig. 4.15). While calculating the deformation field from each template to different gender brains, magnitude or variance of nonlinear deformation field on same voxel of every brain were recorded. Then we calculated the mean or variance of the recorded values for every voxel. Finally, a brain volume that its voxel value represents mean value of magnitude on same voxel was generated. Here we observed the distribution of nonlinear deformation magnitude or variance of both the unbiased bisexual template and the male template. Similarly,

	Template		
	Bisexual template	Male template	Female template
Male	0.8514	0.6574	-
Female	0.9347	-	1.0088

Table 4.8: **The average magnitude of nonlinear deformation comparing Bisexual template, Male template, and Female template.** The average magnitude of nonlinear deformation from male or female subjects to both the unbiased template, created from both gender subjects, and their own gender template were listed.

	Template		
	Bisexual template	Male template	Female template
Male	0.7637	0.4824	-
Female	0.8808	-	0.6527

Table 4.9: **The variance of nonlinear deformation magnitude comparing Bisexual template, Male template, and Female template.** The variance of nonlinear deformation magnitude from male or female subjects to both the unbiased template, created from both gender subjects, and their own gender template were listed.

we examined the distribution of nonlinear deformation magnitude or variance which were calculated from female subjects to the bisexual template and the female emplate.

4.3.2 Similarity between Registered Subjects and Templates

For the anatomical evaluation, we studied the similarity between the template and the images after normalization. We compared the accuracy of normalization of all images of a study-specific group using different templates.

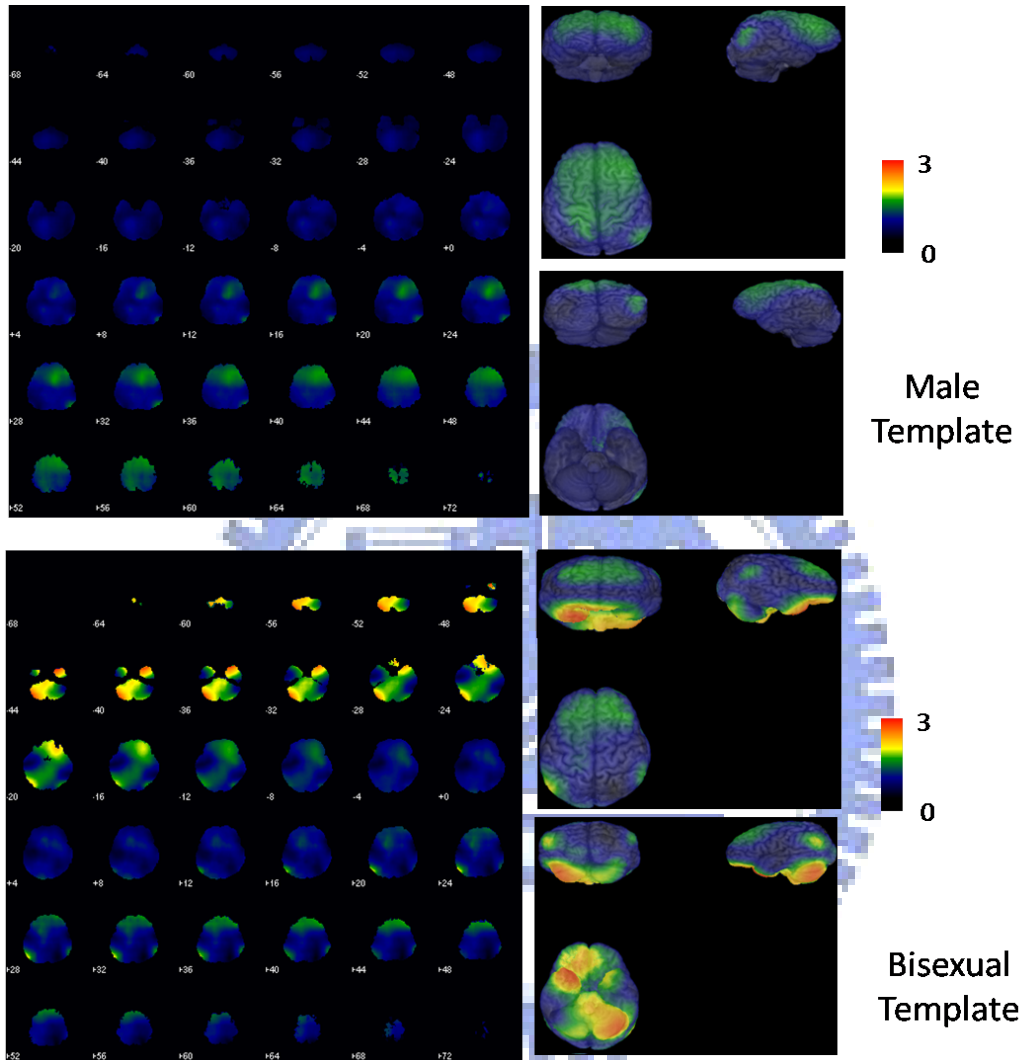


Figure 4.12: **The distribution of nonlinear deformation magnitude to the bisexual template and the male template.** We normalized 57 male subjects to both the the bisexual template and the male template. We averaged the magnitude of nonlinear deformation on the same voxel of each brain. Then, the brain volume that its voxel value represents the mean of the nonlinear deformation was formed. The left figure showed the distribution on slices in axial view.

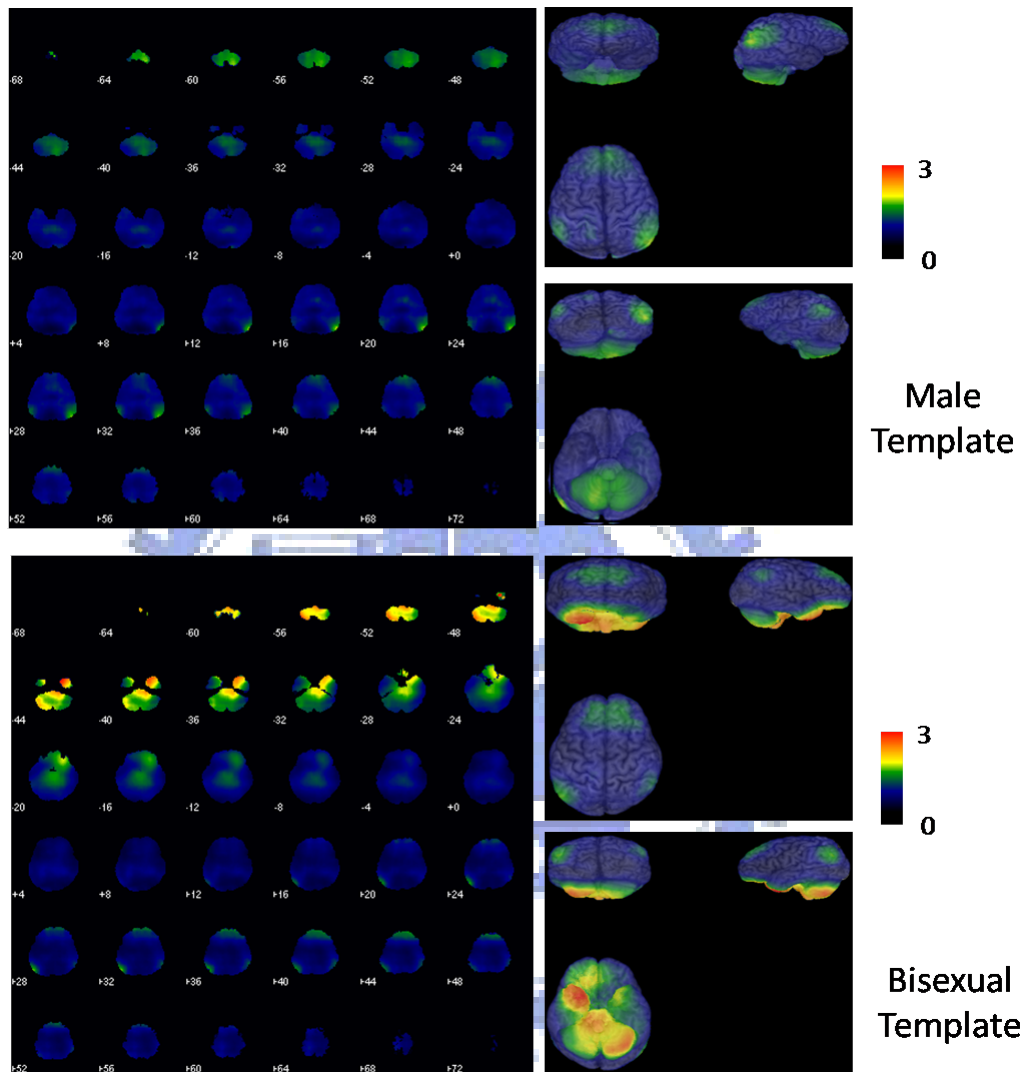


Figure 4.13: **The distribution of nonlinear deformation variance to the bisexual template and the male template.** We normalized 57 male subjects to both the the bisexual template and the male template. We calculated the variance of nonlinear deformation on the same voxel of each brain. Then, the brain volume that its voxel value represents the variance of the nonlinear deformation was formed. The left figure showed the distribution on slices in axial view.

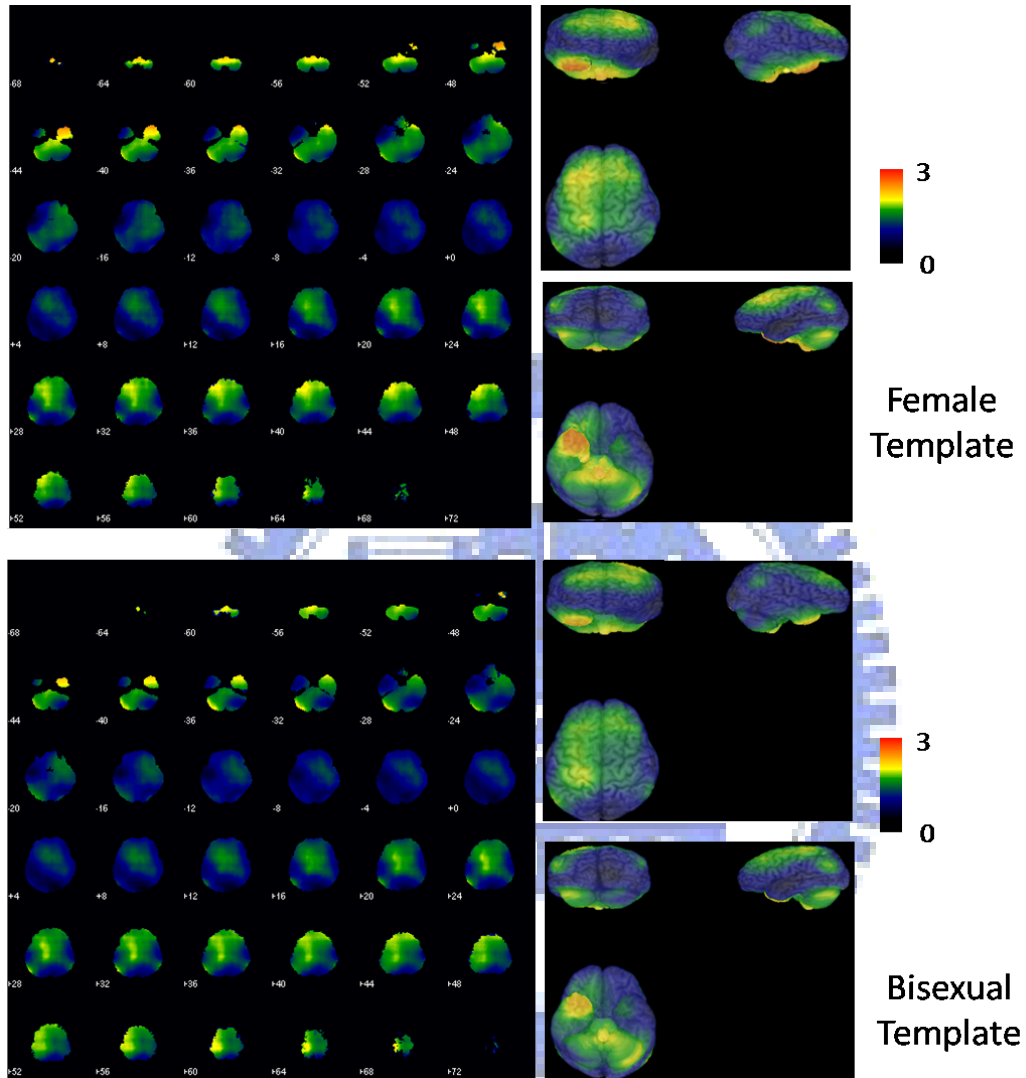


Figure 4.14: **The distribution of nonlinear deformation magnitude to the bisexual template and the female template.** We normalized 69 female subjects to both the the bisexual template and the female template. We averaged the magnitude of nonlinear deformation on the same voxel of each brain. Then, the brain volume that its voxel value represents the mean of the nonlinear deformation was formed. The left figure showed the distribution on slices in axial view.

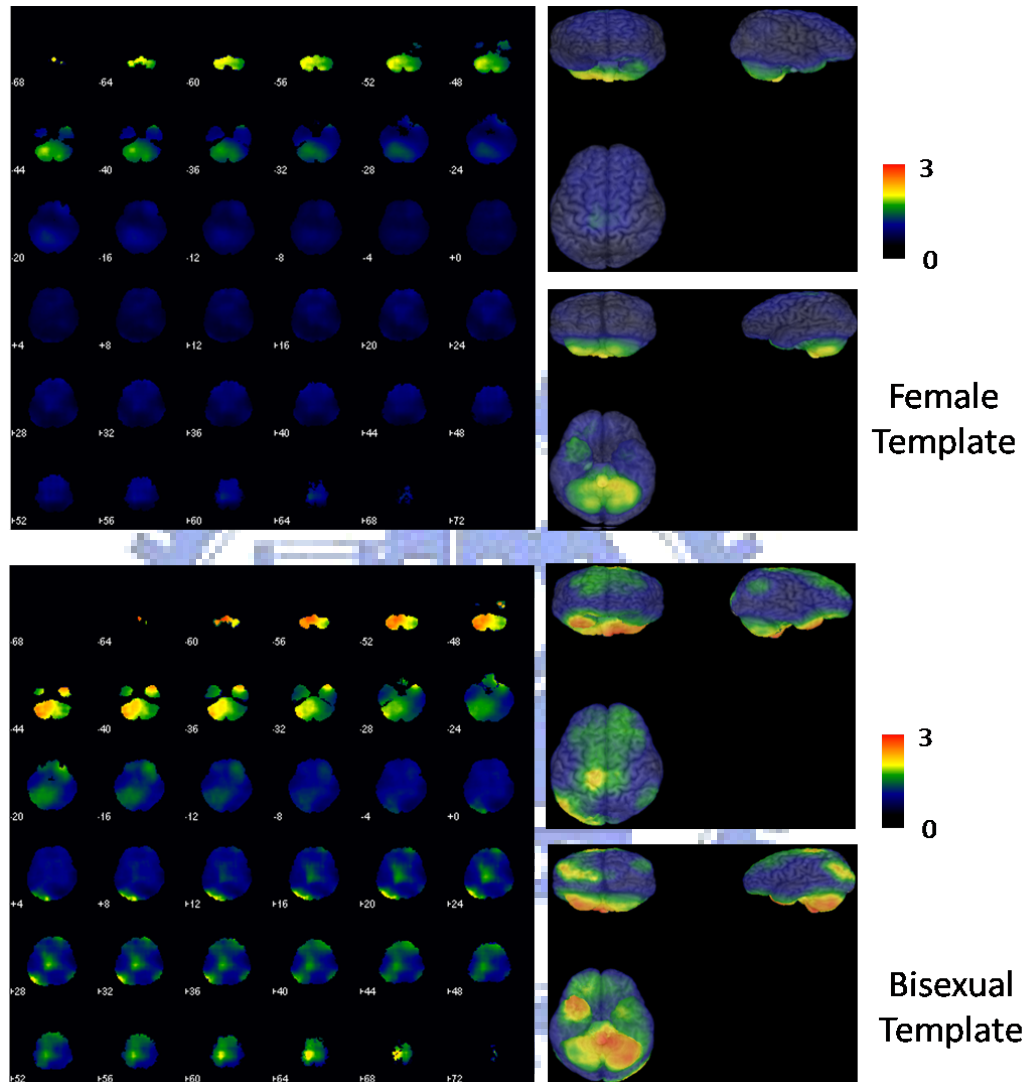


Figure 4.15: **The distribution of nonlinear deformation variance to the bisexual template and the female template.** We normalized 69 female subjects to both the the bisexual template and the female template. We calculated the variance of nonlinear deformation on the same voxel of each brain. Then, the brain volume that its voxel value represents the variance of the nonlinear deformation was formed. The left figure showed the distribution on slices in axial view.

We normalized all 191 brains in our database to the average template, constructed by these 191 brains, and to ICBM152 template. We calculated the correlation ratio (CR) of all normalized brains and the template. The average CR, which represents the similarity between a template and every normalized brains, was listed in Table 4.10.

	Template	
	191 average template	ICBM152
CR	0.8734	0.8339
Std.	0.0245	0.0347

Table 4.10: **The average correlation ratio to 191 average template and ICBM152 template.**

We normalized male or female brains to the bisexual template and male or female template. We calculated the correlation ratio (CR) of normalized brains and the template. The average CR, which represents the similarity between a template and every normalized brains, was listed in Table 4.11.

	Template		
	Bisexual template	Male template	Female template
Male	0.8647	0.8776	-
Female	0.8845	-	0.8868

Table 4.11: **The average correlation ratio to Bisexual average template and gender templates.**

Tissue Name	Labeled Position
Anterior commissure (AC)	Superior and posterior margin
Posterior commissure (PC)	Inferior margin
Anterior corpus callosum (ACC)	Anterior margin
Genu (GU)	Inferior margin
Cerebellar (CB)	Superior margin

Table 4.12: The labeled position of landmarks.

4.4 Mapping to Talairach Coordinate System

We manually identified five tissue landmarks, and recorded their coordinates in the prime template. The labeled position of these five landmarks are listed in Table 4.12. The five landmarks are also labeled in Talairach atlas [29] which is shown in Fig. 4.16.

We recorded the coordinates of the landmarks in the prime template and used our provided tool to transform into Talairach coordinate system. The original position of landmarks in our template space are shown in Fig. 4.17

The original coordinates of landmarks in our template space, the derived mapping coordinates in Talairach space and the actual coordinates in Talairach atlas (ground truth) are shown in Table 4.13.

However, we also transformed the coordinates of five landmarks in Talairach space to our template space. The mapping position are shown in Fig. 4.18.

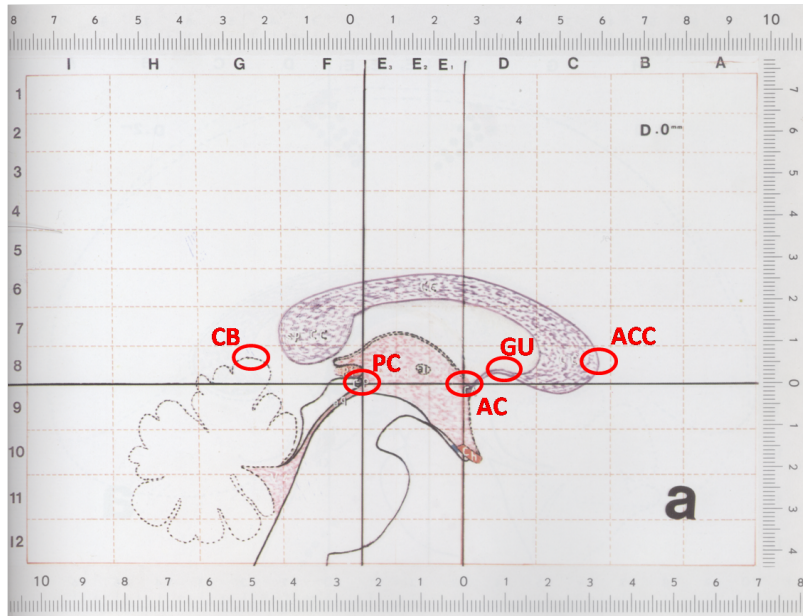


Figure 4.16: **The position of five landmarks in Talairach atlas.** We identified the five landmarks, AC, PC, ACC, GU and CB, in Talairach atlas.

Tissue Name	Labeled position(mm)	Derived position(mm)	Ground truth(mm)
AC	(134.6,127.5,93.0)	(0.4,0.3,-1.6)	(0,0,0)
PC	(134.6,101.0,91.5)	(0.3,-28.3,-1.0)	(0,-24,0)
ACC	(134.6,155.0,93.0)	(0.5,30.1,0.2)	(0,32,4)
GU	(134.6,136.7,94.5)	(0.4,10.4,-1.0)	(0,10,3)
CB	(134.6, 76.5,94.5)	(0.1,-54.8,3.6)	(0,-50,5)

Table 4.13: **The labeled position of landmarks.**

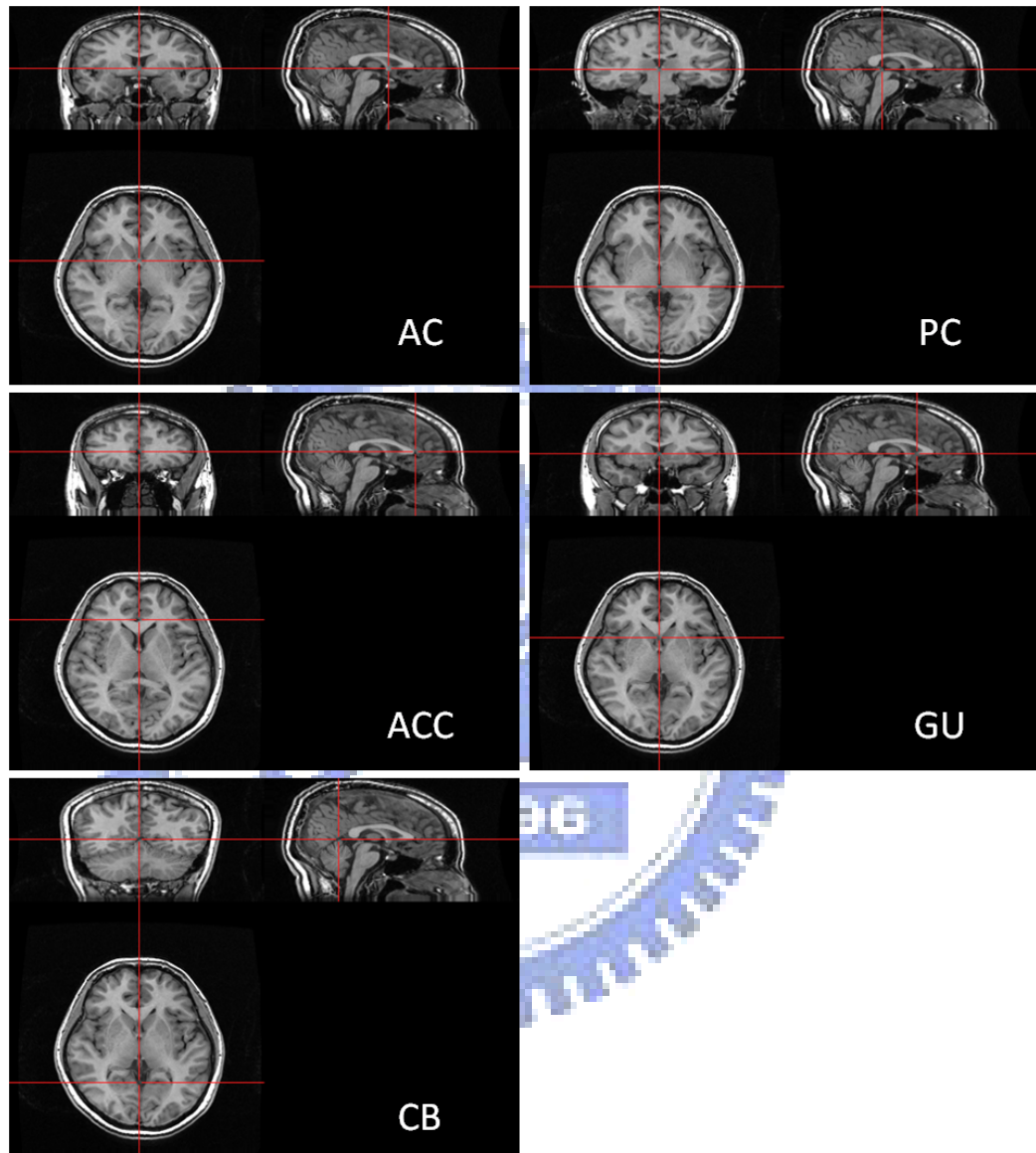


Figure 4.17: **The position of five landmarks in our prime template space.** We identified the five landmarks, AC, PC, ACC, GU and CB, in our prime template space.

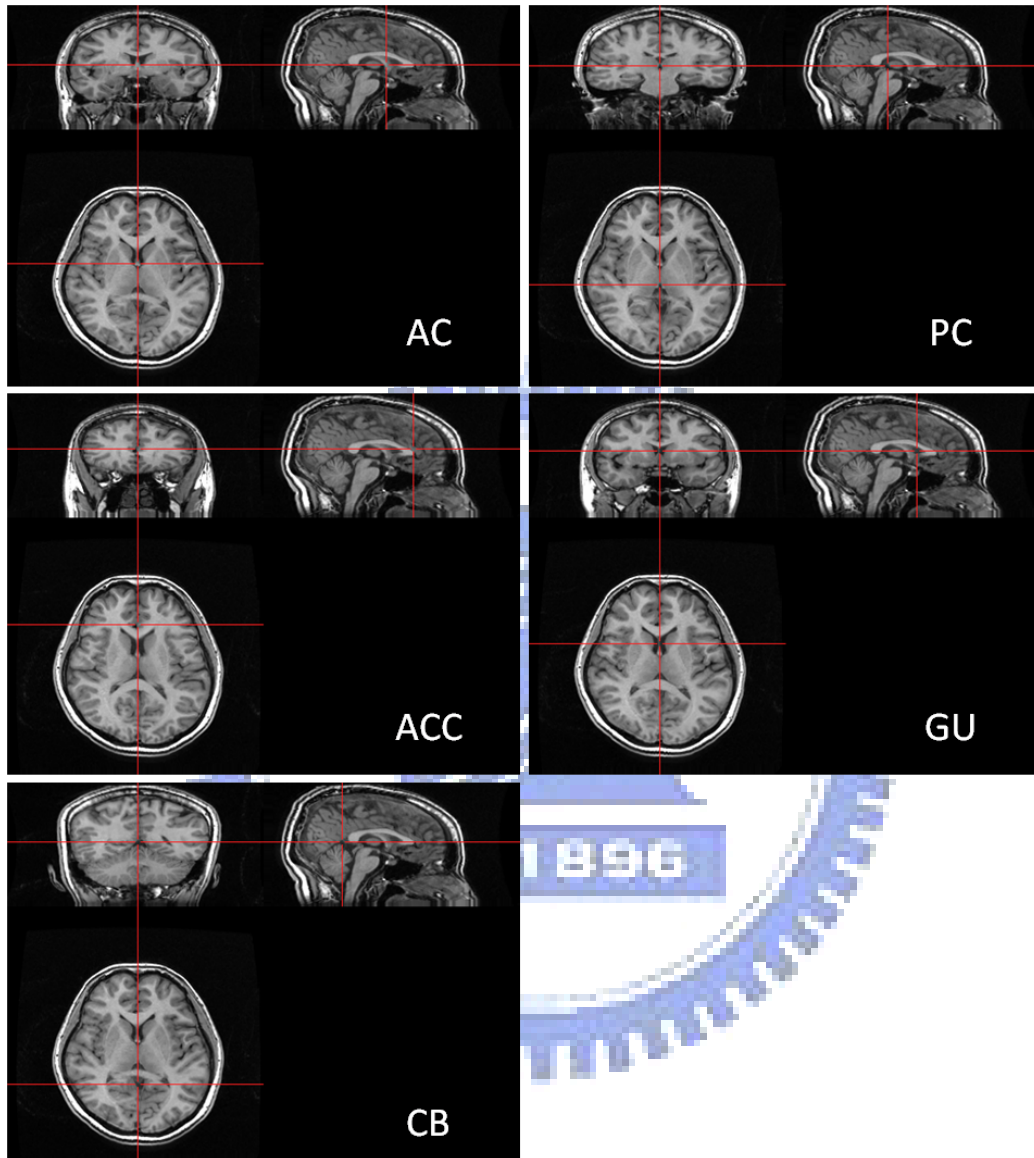


Figure 4.18: **The mapping position of landmarks from Talairach to our template space.** We transformed the five landmarks, AC, PC, ACC, GU and CB, in Talairach coordinate system to our prime template space. These figures show the mapping position in our template space.

Chapter 5

Discussion



5.1 Comparison between Unbiased Template and ICBM152

In this section, we compared the study group specific template which was constructed from all 191 subjects in our database with the ICBM152 template. We evaluated the templates with deformation magnitude, deformation variance and correlation ratio between subjects and each template. In these evaluation experiments, we considered that the unbiased template constructed from 191 Taiwanese subjects is more suitable for Taiwanese than ICBM152 template.

5.1.1 Deformation Field from Individual Brains to Templates

A good template should cause distortion of deformation as small as possible because large deformation may raise registration inaccuracy. Therefore, magnitude of deformation field is a good way to measure the distortion. This evaluation aimed to study the amount of local nonlinear deformation, dismissed the difference of brain size and orientation, needed to perform the normalization. A small total amount of these local changes indicates a small overall difference in brain structure between images and template [15].

We normalized all subjects, 191 subjects in our database, to the average template constructed from these 191 subjects and the ICBM152 template. The nonlinear deformation field was calculated as the distance between corresponding points in the template and the original image after affine transformation. We averaged the magnitude of nonlinear deformation vectors for overall voxels of each individual brain. The magnitude of nonlinear deformation field between subjects and templates was shown in Table 4.5. The AD between subjects and the unbiased template is 1.7556. However, the AD between subjects and ICBM152 template is 2.4572. We found that the unbiased template significantly make less normalization distortion for 191 subjects in this study than ICBM152.

Otherwise, we displayed the distribution of regional nonlinear deformation magnitude in brain region of both the unbiased template and ICBM152. After we calculated the deformation field from each template to 191 individual brains, the magnitude of nonlinear deformation field on same voxel of every brain were recorded. Then we calculated the mean of the recorded values for every voxel. Finally, a brain volume that its voxel value represents mean value of magnitude on same voxel was generated. The more distortion region was represented with the higher value.

Fig. 4.8 shows the distribution of regional nonlinear deformation magnitude in brain region of both the unbiased template and ICBM152. It is obviously to see that the mean magnitude of 191 individual brains represent small-value on the overall brain. However, the large normalization distortion between Taiwanese subjects and ICBM152 is in the inferior region and superior region of the brain. In the other hand, as warping the individual brain to the unbiased template, the significant normalization distortion area is occurred on temporal lobe and cerebellum.

We also calculated the variance of deformation of these two templates. We normalized the 191 brains to the unbiased template and ICBM152. The magnitude deformation vector in each voxel was recorded in the 191 deformation field. Then we calculated the variance of the recorded values for every voxel. Finally, a brain volume that its voxel value represents the variance of deformation vector on same voxel was generated.

By observing the variance of nonlinear deformation field, we can know the anatomically regional variability of the difference between the template and individual brains. Fig. 4.9 shows the distribution of regional nonlinear deformation variance in brain region of both the unbiased template and ICBM152. It is clear to see that the difference between the template and individual brains increases when subjects are normalized to ICBM152 template. In other words, there is more biased between ICBM152 template and individual brains, while normalizing 191 Taiwanese subjects to it; the study specific template which con-

structed from this study group results less bias. The significant region variation occurred in the inferior, including cerebellum, and superior region as normalizing 191 subjects to ICBM152 template. However, the variance distributes smoothly while normalizing 191 subjects to their study-specific unbiased template.

Besides, in order to evaluate the unbiased template with ICBM152 disinterestedly, we used 65 elder subjects, age range is from 36 to 69, in our database as the testing data. We normalized these 65 subjects to the prime-age template, which was constructed by 126 prime-age subjects, age range is from 18 to 35. In this case, the prime-age unbiased template was not consisted of any testing data. In the other hand, we also normalized these 65 subjects to ICBM152. The AD (Table 4.6) between 65 subjects and the unbiased prime-age template is 0.8215 in contrast with 1.9907 with ICBM152 participated. In the distribution of magnitude or variance of nonlinear deformation, we can see that much less deformation magnitude and variance are introduced when the 65 elder subjects were normalized to unbiased prime-age template.

5.1.2 Correlation Ratio between Subjects and Templates

The deformation magnitude only provides the amount of normalization distortion. However, the less distortion can not imply the higher registration accuracy. For this reason, we tried to compare the accuracy of normalization of all 191 subject brain images using both the unbiased template and ICBM152 template for the anatomical evaluation. We studied the similarity between the templates and the images after normalization by correlation ratio (CR).

The correlation ratio, introduced by Roche, A. et al. in 1998 [24], provided the similarity measure for MR images. We normalized all 191 brain images to the unbiased template or ICBM152 template and calculated the average of correlation ratio between them. The larger correlation ratio is, the similar the template and warped images are. The results of

CR between 191 warped images and the templates are shown in Table 4.10. The CR between warped images and the unbiased template is 0.8734 and between warped images and ICBM152 template is 0.8339. The result evidently reveals the unbiased template for this study group improves the registration accuracy.

5.2 Comparison between Bisexual Template and Gender Template

In this section, we evaluated the study specific templates for both gender groups. The template construction procedure was applied on the male and female population, 57 males and 69 females. Also we constructed the bisexual template including both gender groups. The results revealed that the study specific template is more suitable for the study group.

5.2.1 Deformation Field from Individual Brains to Templates

This evaluation aimed to study the amount of local nonlinear deformation, dismissed the difference of brain size and orientation, needed to perform the normalization. We normalized male subjects, 57 subjects in our database, to the unbiased template constructed from these 57 male subjects and obtained the nonlinear deformation field. In the other hand, we normalized male subject brains to the bisexual template constructed from both male and female subjects and derived the nonlinear deformation. We also normalized 69 female subjects to both female template and bisexual template as mentioned above.

We averaged the magnitude of nonlinear deformation vectors for overall voxels and the magnitude of nonlinear deformation field between subjects and templates was shown in Table 4.8. The AD between male subjects and the bisexual template is 0.8514. However, the

AD between male subjects and male template is 0.6574. It is clear to see that the male template significantly make less normalization distortion for male subjects in this study than the bisexual template. However, in the experiment for female subjects, the AD between female subjects and the bisexual template is 0.9347, and AD between female subjects and female template is 1,0088. Although the AD between female subjects and female template is larger than bisexual template, there is no significant difference.

Fig. 4.12 shows the distribution of regional nonlinear deformation magnitude in brain region of both the male template and the bisexual template. We can see that the deformation magnitude of male brains, as normalized to the male template, represent small value on the inferior region of brain, including temporal lobe and cerebellum.

By observing the variance of nonlinear deformation field, we can know the anatomically regional variability of individual brain. Fig. 4.13 shows the distribution of regional nonlinear deformation variance in brain region of both the male template and the bisexual template. The region of variation between individual brains occur superior prefrontal region in both the male template and the bisexual template. However, the bisexual template results more normalization distortion in left cerebellum region and right temporal lobe while normalizing male subjects to it.

Fig. 4.14 shows the distribution of regional nonlinear deformation magnitude in brain region of both the female template and the bisexual template. We can see that the deformation magnitude of female brains reveals higher value in the right temporal lobe when both the female template and bisexual template participated. There is no significant difference of nonlinear deformation between the female template and bisexual template.

Fig. 4.15 shows the distribution of regional nonlinear deformation variance in brain region of both the female template and the bisexual template. The region of variation be-

tween individual brains occurs in cerebellum region in both the female template and the bisexual template. However, the bisexual template results more normalization distortion in cerebellum and occipital region while normalizing female subjects to it. The female template causes less variance of nonlinear deformation for female subjects.

5.2.2 Correlation Ratio between Subjects and Templates

We calculate the correlation ration between warped images and the template to evaluate the similarity of them. In other words, we study the performance of registration when different templates participate. The results of CR between warped images in both gender group and the bisexual template are shown in Table 4.11. The CR between warped male images and the male template is 0.8776 and between warped male images and the bisexual template is 0.8647. Otherwise, the CR between warped female images and the female template is 0.8868 and between warped female images and the bisexual template is 0.8845. The result reveals the gender templates for the subjects in their group participated improves the registration accuracy.

5.3 Mapping to Talairach Coordinate System

In order to verify the mapping coordinate in Talairach coordinate system from our template space, we manually identified five tissue landmarks and transform them to Talairach space. The labeled position of these five landmarks, including AC, PC, ACC, GU and CB, are listed in Table 4.12. We located these landmarks in Talairach atlas to acquire the ground truth. Fig. 4.16 shows the coordinates of the landmarks in Talairach atlas. Fig. 4.17 demonstrates the position of the five landmarks in our unbiased prime template.

We used the proposed method, which used MNI template as the bridge, to convert the coordinates from our template space to Talairach space. Table 4.13 shows the original coordinates in our template space, the derived mapping coordinates and the real coordinates in Talairach space (the ground truth). However, due to the artifact of manual identification of landmarks and transformation error from MNI to Talairach space, the derived mapping coordinates are not identical to the real coordinates in Talairach coordinates. Even though, the results are still promising when the transformation from MNI space to Talairach space advances [5].



Chapter 6

Conclusions

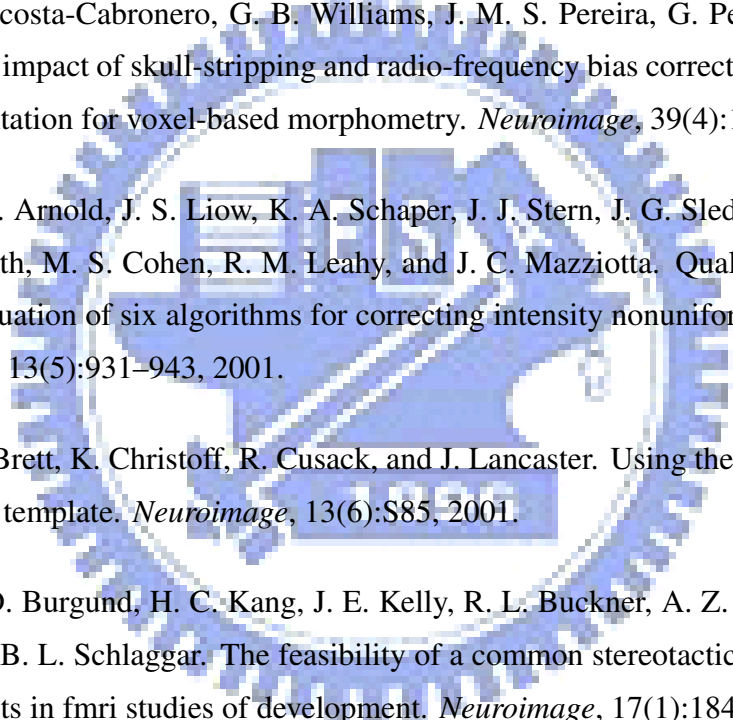


In this study, we developed an automatic procedure of constructing MRI brain templates and provided the transformation from our template space to Talairach space. The construction procedure contained selection of representative brain and determination of unbiased stereotaxic space. First, because we need a reference space to derive template space, we chose a brain volume, which is one subject of the image set and has the minimum variation of deformation magnitude to the other subjects, as the representative brain. Second, we computed the unbiased space according to the representative brain and all other brain images. In this step, we developed an interpolation algorithm to calculate the corresponding position from the template space to the space of the representative brain. Besides, in order to obtain the structural and functional labels, we also provided the transformation from our template to the Talairach coordinate system.

It is important to have a brain template for functional and structure researches. Brain comparison, based on normalizing to a standard brain template, needs a suitable template which diminishes the distortion of normalization and improves the registration accuracy. In this study, we compared the study specific unbiased template, which was constructed from 191 Taiwanese brains, and ICBM152 template. The results revealed that the unbiased template could diminish the nonlinear deformation and improved the registration accuracy evidently.

To evaluate the performance of using the study specific template, we applied our procedure to construct the templates for both gender groups. We compared the gender templates with the bisexual template. The observation from this study showed that the study specific templates improved the registration accuracy. Thus, we may conclude that the study specific unbiased template is more suitable for the subjects in this study group.

Bibliography

- 
- [1] J. Acosta-Cabronero, G. B. Williams, J. M. S. Pereira, G. Pengas, and P. J. Nestor. The impact of skull-stripping and radio-frequency bias correction on grey-matter segmentation for voxel-based morphometry. *Neuroimage*, 39(4):1654–1665, 2008.
- [2] J. B. Arnold, J. S. Liow, K. A. Schaper, J. J. Stern, J. G. Sled, D. W. Shattuck, A. J. Worth, M. S. Cohen, R. M. Leahy, and J. C. Mazziotta. Qualitative and quantitative evaluation of six algorithms for correcting intensity nonuniformity effects. *Neuroimage*, 13(5):931–943, 2001.
- [3] M. Brett, K. Christoff, R. Cusack, and J. Lancaster. Using the talairach atlas with the mni template. *Neuroimage*, 13(6):S85, 2001.
- [4] E. D. Burgund, H. C. Kang, J. E. Kelly, R. L. Buckner, A. Z. Snyder, S. E. Petersen, and B. L. Schlaggar. The feasibility of a common stereotactic space for children and adults in fmri studies of development. *Neuroimage*, 17(1):184–200, 2002.
- [5] P. S. Carmack, J. Spence, R. F. Gunst, W. R. Schucany, W. A. Woodward, and R. W. Haley. Improved agreement between talairach and mni coordinate spaces in deep brain regions. *Neuroimage*, 22(1):367–371, 2004.
- [6] W. Chau and A. R. McIntosh. The talairach coordinate of a point in the mni space: how to interpret it. *Neuroimage*, 25(2):408–416, 2005.
- [7] D. L. Collins, T. M. Peters, and A. C. Evans. Automated 3d nonlinear deformation

- procedure for determination of gross morphometric variability in human brain. *Proceedings of SPIE*, 2359:180, 2003.
- [8] J. Diedrichsen. A spatially unbiased atlas template of the human cerebellum. *Neuroimage*, 33(1):127–138, 2006.
- [9] A. C. Evans, D. L. Collins, S. R. Mills, E. D. Brown, R. L. Kelly, and T. M. Peters. 3d statistical neuroanatomical models from 305 mri volumes. *Nuclear Science Symposium and Medical Imaging Conference, 1993., 1993 IEEE Conference Record.*, pages 1813–1817, 1993.
- [10] A. Gholipour, N. Kehtarnavaz, R. Briggs, M. Devous, and K. Gopinath. Brain functional localization: A survey of image registration techniques. *Medical Imaging, IEEE Transactions on*, 26(4):427–451, 2007.
- [11] J. D. Gispert, J. Pascau, S. Reig, R. Martinez-Lazaro, V. Molina, P. Garcia-Barreno, and M. Desco. Influence of the normalization template on the outcome of statistical parametric mapping of pet scans. *Neuroimage*, 19(3):601–612, 2003.
- [12] A. Guimond, J. Meunier, and J. P. Thirion. Average brain models: A convergence study. *Computer Vision and Image Understanding*, 77(2):192–210, 2000.
- [13] A. Huang, R. Abugharbieh, R. Tam, and A. Traboulsee. Automatic mri brain tissue segmentation using a hybrid statistical and geometric model. *3rd IEEE International Symposium on Biomedical Imaging, April*, 2006.
- [14] S. Joshi, B. Davis, M. Jomier, and G. Gerig. Unbiased diffeomorphic atlas construction for computational anatomy. *Neuroimage*, 23:151–160, 2004.
- [15] K. Kazemi, H. A. Moghaddam, R. Grebe, C. Gondry-Jouet, and F. Wallois. A neonatal atlas template for spatial normalization of whole-brain magnetic resonance images of newborns: Preliminary results. *Neuroimage*, 37(2):463–473, 2007.
- [16] P. Kochunov, J. Lancaster, P. Thompson, A. W. Toga, P. Brewer, J. Hardies, and P. Fox. An optimized individual target brain in the talairach coordinate system. *Neuroimage*, 17(2):922–927, 2002.

- [17] J. S. Lee, D. S. Lee, J. Kim, Y. K. Kim, E. Kang, H. Kang, K. W. Kang, J. M. Lee, J. J. Kim, and H. J. Park. Development of korean standard brain templates. *J Korean Med Sci*, 20(3):483–488, 2005.
- [18] Jia-Xiu Liu, Yong-Sheng Chen, and Li-Fen Chen. Affine and nonlinear spatial normalization techniques using derivatives of brain magnetic resonance images. In *Annual Meeting of the Organization for Human Brain Mapping*, Austria, 2008.
- [19] J. D. MacDonald. *A method for identifying geometrically simple surfaces from three-dimensional images*. PhD thesis, McGill University, 2000.
- [20] J. C. Mazziotta, A. W. Toga, A. Evans, P. Fox, and J. Lancaster. A probabilistic atlas of the human brain: Theory and rationale for its development the international consortium for brain mapping (icbm). *Neuroimage*, 2(2PA):89–101, 1995.
- [21] J. C. Mazziotta, A. W. Toga, A. Evans, P. Fox, and J. Lancaster. A probabilistic atlas of the human brain: International consortium for brain mapping (icbm). *Philosophical Transactions of the Royal Society B: Biological Sciences*, 356(1412):1293–1322, 2001.
- [22] O. Muzik, D. C. Chugani, C. Juhasz, C. Shen, and H. T. Chugani. Statistical parametric mapping: Assessment of application in children. *Neuroimage*, 12(5):538–549, 2000.
- [23] S. Prima, S. Ourselin, and N. Ayache. Computation of the mid-sagittal plane in 3-d brain images. *Medical Imaging, IEEE Transactions on*, 21(2):122–138, 2002.
- [24] A. Roche, G. Malandain, X. Pennec, and N. Ayache. The correlation ratio as a new similarity measure for multimodal image registration. *Proc. MICCAI*, 98:1115–1124, 1998.
- [25] P. E. Roland and K. Zilles. Brain atlases—a new research tool. *Trends Neurosci*, 17(11):458–67, 1994.

- [26] J. G. Sled, A. P. Zijdenbos, and A. C. Evans. A nonparametric method for automatic correction of intensity nonuniformity in mri data. *Medical Imaging, IEEE Transactions on*, 17(1):87–97, 1998.
- [27] S. M. Smith, M. Jenkinson, M. W. Woolrich, C. F. Beckmann, T. E. J. Behrens, H. Johansen-Berg, P. R. Bannister, M. De Luca, I. Drobnjak, and D. E. Flitney. Advances in functional and structural mr image analysis and implementation as fsl. *Neuroimage*, 23:208–219, 2004.
- [28] J. Talairach and P. Tournoux. Co-planar stereotaxic atlas of a human brain: 3-dimensional proportional system an approach to cerebral imaging. *Thieme Medical Publishers*, 1988.
- [29] J. Talairach and P. Tournoux. *Co-Planar Stereotaxic Atlas of the Human Brain: 3-Dimensional Proportional System: An Approach to Cerebral Imaging*. Thieme, 1988.
- [30] P. M. Thompson, C. Schwartz, and A. W. Toga. High-resolution random mesh algorithms for creating a probabilistic 3d surface atlas of the human brain. *Neuroimage*, 3(1):19–34, 1996.
- [31] P. M. Thompson and A. W. Toga. Detection, visualization and animation of abnormal anatomic structure with a deformable probabilistic brain atlas based on random vector field transformations. *Medical Image Analysis*, 1(4):271–294, 1997.
- [32] P. M. Thompson, R. P. Woods, M. S. Mega, and A. W. Toga. Mathematical/computational challenges in creating deformable and probabilistic atlases of the human brain. *Human Brain Mapping*, 9(2):81–92, 2000.
- [33] D. C. Van Essen. A population-average, landmark-and surface-based (pals) atlas of human cerebral cortex. *Neuroimage*, 28(3):635–662, 2005.
- [34] A. P. Zijdenbos and B. M. Dawant. Brain segmentation and white matter lesion detection in mr images. *Crit Rev Biomed Eng*, 22(5-6):401–65, 1994.

- [35] K. Zilles, R. Kawashima, A. Dabringhaus, H. Fukuda, and T. Schormann. Hemispheric shape of european and japanese brains: 3d mri analysis of intersubject variability, ethnical, and gender differences. *Neuroimage*, 13(2):262–271, 2001.

